# แบบจำลองการแพร่สำหรับการปลูกผลึกด้วยการคัดเลือกพื้นที่ของคิวบิกแกลเลียมไนไตรด์โดยกระบวนการเอ็มโอวีพีอี

นางสาวพิชญ์สิริ สุกแก้ว



วิทยานิพนธ์นี้เป็นส่วนหนึ่งของการศึกษาตามหลักสูตรปริญญาวิทยาศาสตรมหาบัณฑิต
สาขาวิชาฟิสิกส์ ภาควิชาฟิสิกส์
คณะวิทยาศาสตร์ จุฬาลงกรณ์มหาวิทยาลัย
ปีการศึกษา 2552

# DIFFUSION MODEL FOR SELECTIVE AREA GROWTH OF CUBIC GaN UNDER MOVPE PROCESS

Miss Pitsiri Sukkaew



A Thesis Submitted in Partial Fulfillment of the Requirements
for the Degree of Master of Science Program in Physics

Department of Physics

Faculty of Science

Chulalongkorn University

Academic Year 2009

| | |
|---|---|
| Thesis Title | DIFFUSION MODEL FOR SELECTIVE AREA GROWTH OF CUBIC GaN UNDER MOVPE PROCESS |
| By | Miss Pitsiri Sukkaew |
| Field of Study | Physics |
| Thesis Advisor | Assistant Professor Sakuntam Sanorpim, Ph.D. |

---

Accepted by the Faculty of Science, Chulalongkorn University in Partial Fulfillment of the Requirements for the Master's Degree

..... Dean of the Faculty of Science
(Professor Supot Hannongbua, Ph.D.)

THESIS COMMITTEE

..... Chairman
(Associate Professor Udomsilp Pinsook, Ph.D.)

..... Thesis Advisor
(Assistant Professor Sakuntam Sanorpim, Ph.D.)

..... Examiner
(Assistant Professor Sukkaneste Tungasmita, Ph.D.)

..... External Examiner
(Supitch Khemmani, Ph.D.)

พิชญ์สิริ สุกแก้ว: แบบจำลองการแพร่สำหรับการปลูกผลึกด้วยการคัดเลือกพื้นที่ของคิวบิกแกลเลียมไนไตรด์โดยกระบวนการเอ็มโอวีพีอี (DIFFUSION MODEL FOR SELECTIVE AREA GROWTH OF CUBIC GaN UNDER MOVPE PROCESS). อาจารย์ที่ปรึกษาวิทยานิพนธ์: ผศ.ดร. สกุลธรรม เสนาะพิมพ์, 74 หน้า

ผู้วิจัยได้ประยุกต์ใช้แบบจำลองการแพร่ในการอธิบายโพรไฟล์ความหนาและสัณฐานวิทยาของฟิล์มชนิดคิวบิกแกลเลียมไนไตรด์ซึ่งทำการปลูกผลึกด้วยการคัดเลือกพื้นที่ ภายใต้กระบวนการเมทอล-ออแกนิกเวเปอร์เฟสเอพิเทกซี โดยมีบริเวณเปิดบนพื้นผิวแคบ ผลการศึกษาพบว่า แบบจำลองการแพร่ในสถานะก๊าซ (vapor phase diffusion model) สามารถอธิบายโพรไฟล์ความหนาที่ค่าตัวประกอบเติมเต็ม (Fill Factor) มากกว่า 0.5 ได้เป็นอย่างดีที่ค่า $D/k$ ซึ่งเป็นอัตราส่วนระหว่างค่าสัมประสิทธิ์การแพร่ต่ออัตราการทับถมเป็น 15 ไมโครเมตร สำหรับโพรไฟล์ในช่วงค่าตัวประกอบเติมเต็มน้อยกว่า 0.5 ผลการจำลองมีค่าต่ำกว่าค่าที่ได้ผลการทดลอง และพบว่าแบบจำลองดังกล่าวไม่สามารถอธิบายลักษณะทางสัณฐานวิทยาของฟิล์มซึ่งมีการตรวจพบอัตราการปลูกที่สูงผิดปกติที่บริเวณขอบซึ่งเป็นรอยต่อระหว่างระนาบ (111)B และ (001) ซึ่งผู้วิจัยได้ตั้งสมมติฐาน ว่าเป็นผลมาจากการละการพิจารณาผลของกระบวนการไมเกรชันบนพื้นผิว (surface migration process) เพื่อทดสอบสมมติฐานดังกล่าว ผู้วิจัยได้เพิ่มผลจากแบบจำลองไมเกรชันบนพื้นผิว (surface migration model) เข้ากับผลจากแบบจำลองก่อนหน้า พบว่าสามารถอธิบายโพรไฟล์ความหนาในช่วงค่าตัวประกอบเติมเต็มน้อยกว่า 0.5 ได้เป็นอย่างดีที่ค่าความยาวไมเกรชันบนพื้นผิว (surface migration length) และค่าการถ่วงน้ำหนักของการเพิ่มเข้าของไมเกรชันบนพื้นผิว (weight of surface migration contribution) เป็น 0.8 ไมโครเมตรและ 0.03 ต่อนาทีตามลำดับ นอกจากนี้ ยังสามารถอธิบายการเกิดขึ้นของอัตราการปลูกที่สูงผิดปกติที่บริเวณขอบ ซึ่งนำไปสู่การทำนายสภาวะการปลูกซึ่งสามารถลดการก่อเกิดของโครงสร้างแบบเฮกซะกอนัล ( hexagonal) ได้

ภาควิชา : ฟิสิกส์ ลายมือชื่อนิสิต พิชญ์สิริ สุกแก้ว

สาขาวิชา : ฟิสิกส์ ลายมือชื่ออาจารย์ที่ปรึกษา

ปีการศึกษา : 2552

## 5072389423 : MAJOR PHYSICS

KEYWORDS : Vapor phase diffusion model/ surface migration model/ selective area growth/ metalorganic vapor phase eptiaxy/ cubic GaN

PITSIRI SUKKAEW: DIFFUSION MODEL FOR SELECTIVE AREA GROWTH OF CUBIC GaN UNDER MOVPE PROCESS. THESIS ADVISOR: [ASSISTANT PROFESSOR SAKUNTAM SANORPIM, Ph.D.], 74 pp.

Diffusion models were applied in order to describe the thickness profiles and morphologies of cubic GaN grown by selective area growth under metalorganic vapor phase epitaxy with narrow open windows. The simulated results from vapor phase diffusion model with $D/k$ - the ratio of diffusion coefficient to the deposition rate constant – of 15 μm was found to agree well with the film thickness profile for fill factor higher than 0.5, while for fill factor lower than 0.5 the predicted values were found to be lower than the experiments. Moreover, the abnormal growth rate occurring at the edge connecting (111)B sidewall facets and (001) plane could not be explained by the simulation results. The inconsistency was believed to result from the lack of the effects from surface migration process. Therefore the results from surface migration model were added to the previous results, and the improvement of the thickness profiles between the simulation and experiment was observed. The experimental profiles with fill factor lower than 0.5 was found to be well fitted with the simulation results with surface migration length and the weight of surface migration contribution of 0.8 μm and 0.03 $min^{-1}$, respectively. Also, the simulation results were able to describe the abnormal growth rate at the edges and consequently suggest a way to reduce hexagonal inclusion which has been observed in c-GaN.

Department : Physics Student's Signature Pitsiri Sukkaew

Field of Study : Physics Advisor's Signature

Academic Year : 2009

# Acknowledgements

I would like to express my deeply gratitude to my advisor, Assistant Professor Dr. Sakuntam Sanorpim, for the willing supports and guidance he has been giving me all through these three years of my study and research. I would also like to thank him for his stimulating suggestions and encouragements which deeply benefited me in all these times, and for his generosity of giving me opportunities to present my work in many national and international conferences. From him, not only the research techniques and backgrounds, I also have learned several of important scientific knowledge such as how to deal with problems in scientific methods, the methods of scientific thinking, making a discussion and drawing a conclusion in order to obtain insight understandings including to obtain further interesting topics of my future research, which will greatly benefit my future study and careers.

I would like to thanks my thesis committee: Assistant Professor Dr. Sukkaneste Tungasmita, Associate Professor Dr. Udomsilp Pinsook and Dr. Supitch Khemmani for giving me helpful comments and suggestions on the thesis. I also wish to thank Professor Dr. Kentaro Onabe from Onabe lab, The University of Tokyo, Japan for providing excellent cubic GaN samples.

I would like to acknowledge the financial supports from Office of the National Research Council of Thailand (NRCT), from Science and Technology Innovation Support Grant, Chulalongkorn University, from CU. Graduate School Thesis Grant, Graduate School, Chulalongkorn University, from The Development and Promotion for Science and Technology Talents Project (DPST) and from Conference Grant for Master Degree Student, the Department of Physics, Faculty of Science, Chulalongkorn University.

My special thanks go to all of my friends and beloved family for being there for me, for cheering me up when I was down, for give me several helpful advices, discussions and supports, and for every joyful moment. I also would like to thanks all members of the Advanced Materials Physics lab both on the 19$^{th}$ floor of MHMK building, the Physics One building, including my Swedish friend for technical and programming supports, for helpful research knowledge and cheerful moments. Thank you all.

# Table of Contents

# List of Tables

# List of Figures

# CHAPTER I
# INTRODUCTION

## 1.1 Overview

GaN is a wide direct band gap semiconductor which has attracted much attention for an application in optoelectronic devices technology [1-3]. The substance is very desirable in the fabrication of blue light emitting diodes (LEDs) and blue ray laser diodes (LDs) [1], used for high density optical storage. It is also utilized for applications under severe conditions such as an operation with high breakdown field [2], high frequency and high temperature [3]. An exploitation of zinc blende (cubic phase) GaN (c-GaN), which is a metastable phase of GaN, benefits the general uses of wurtzite (hexagonal phase) GaN (h-GaN) in many ways. For example, c-GaN can be grown on non-planar (001) cubic substrates such as GaAs (001) [4]. The technology developed for GaAs is therefore applicable. Additionally, compared to wurtzite crystals, zinc blende crystals are easier to be cleaved for laser facets, and also easier doping and contacting in device fabrications [4]. Also, zinc blende structure has higher symmetry than hexagonal structure. Then, superior properties such as higher drift velocity, drift mobility and carrier energy of electrons and holes are expected [5]. Furthermore, c-GaN grown along [001] direction has no spontaneous polarization or piezoelectric field, which affects an efficiency of h-GaN based LEDs structured along the c-axis [6]. Higher efficiency is then expected for an application in quantum optoelectronics. Also, c-GaN quantum wells are predicted to have higher optical gains than those of h-GaN quantum wells over a wide range of carrier density [7]. These advantages brought much interest to the development and quality of c-GaN.

Metal organic vapor phase epitaxy (MOVPE) is a growth method widely used in an industrial production. However, an inclusion of hexagonal phase GaN [8-11], which reduces the quality of light emitting, is usually observed in c-GaN grown films. To improve the crystal quality of c-GaN, selective area metalorganic vapor phase epitaxy (SA-MOVPE) becomes a promising technique. It is known that c-GaN layers grown by SA-MOVPE contain less density of planar defects [12, 13] compared to the layer grown under conventional MOVPE. Another interesting property of SA-MOVPE technique is a selectivity of the growth area. This

technique has been widely utilized in the fabrication of nano-structures such as quantum dots [14, 15] and quantum wires [16]. Moreover, anisotropic growth features were usually observed with different pattern orientations [17, 18]. The method is then attracted attentions among the fabrication of quantum wells, which requires the presence of distinct crystal facets [19]. Besides the observation of anisotropic growth features, the orientations were also found to have effects on the film growth rates both in lateral and vertical directions [20, 21]. Also, the growth rate was found to depend strongly on the fill factor – defined as the ratio of the open width to the pattern period [22, 23]. More interestingly, an abnormal growth rate enhancement was usually found near masks and distinct facets [24]. Therefore, to control the growth under SA-MOVPE, an understanding in the effects of different growth condition is required.

It is known that there are two main mechanisms governing SA-MOVPE, i.e. vapor phase diffusion (VPD) and surface migration (SM). For wide opening width (>10s μm), the VPD effect was found to dominate, and the surface migration effect was negligible [25]. Interestingly, it was observed that, in the case of a layer with (111)B sidewalls, the SM effects made more contributions with an increasing of the thickness [26]. Also, the SM effect becomes less dominant when the length of (111)B facets become larger than a certain value [27]. The SM effect is therefore time dependent. However, all the results mentioned above were focused on selective areas with wide open windows. The surface migration effects in those cases were therefore limited to occur only in the region near the edges of an open window.

In this work, we focus on a selective area growth with narrow open windows (<10 μm) in order to investigate the effects of VPD and SM on the growth features of c-GaN.

## 1.2 Objectives and organization of the thesis

This work aims for an understanding of the growth mechanisms of SA growth via metal organic vapor phase epitaxy. The focus is on the growth features, i.e. morphologies and growth rate of cubic GaN narrow stripes with a few micron width. Two main growth mechanisms in SA growth, namely VPD and SM processes, will be investigated. The final goal is to find the way to control the growth features of c-GaN.

The thesis is organized as follows.

Chapter 2 is a brief review of experimental and theoretical background in SA-MOVPE. The main contents are the details of selective area MOVPE growth method including experimental results of SA c-GaN and the review of diffusion models: VPD and SM models.

Chapter 3 gives details about our experiments and modeling. In the part of experiments, information of the growth system, experimental results and discussion will be provided. In modeling part, the derivations and our modifications of VPD model and SM model will be described.

Chapter 4 gives the results simulated using VPD model. Aspects of diffusion process and the physical meaning of parameters will be drawn and discussed. The morphologies of the actual films and the simulation results will be compared. The growth condition where the surface migration process starts to be noticeable is also given.

Chapter 5 provides the results simulated using VPD model including SM effects. The influence of SM on the thickness and morphologies will be investigated by varying the parameters in SM model. The physical meaning of these parameters will be drawn and interpreted in term of growth conditions.

Finally, Chapter 6 gives the conclusions of the thesis.

# CHAPTER II
# BACKGROUND

In this chapter, a brief review of experimental and theoretical background pertaining to SA-MOVPE is provided. In the first two sections, details of SA-MOVPE growth process and previous experimental results of SA c-GaN films are given. In the last part, a brief review of diffusion models is described. This part is divided into two subsections, which give details of VPD models with and without an addition of surface migration effects respectively.

## 2.1 Selective area MOVPE

MOVPE is a deposition process widely used for an epitaxial film growth, i.e. growing a film layer with a single crystal structure on top of a crystalline substrate. This method has been extensively utilized for an epitaxial growth of III-V semiconductors, such as gallium arsenide (GaAs) and gallium nitride (GaN). Its advantages are, for example, its low growth rate with good uniformity, high flexibility for different growth materials and capable of expanding to commercial production. MOVPE can be also called as metalorganic chemical vapor deposition (MOCVD). Both of these names result from their unique characteristics, i.e. the film constituents, which are metalorganic compounds for group III precursors and

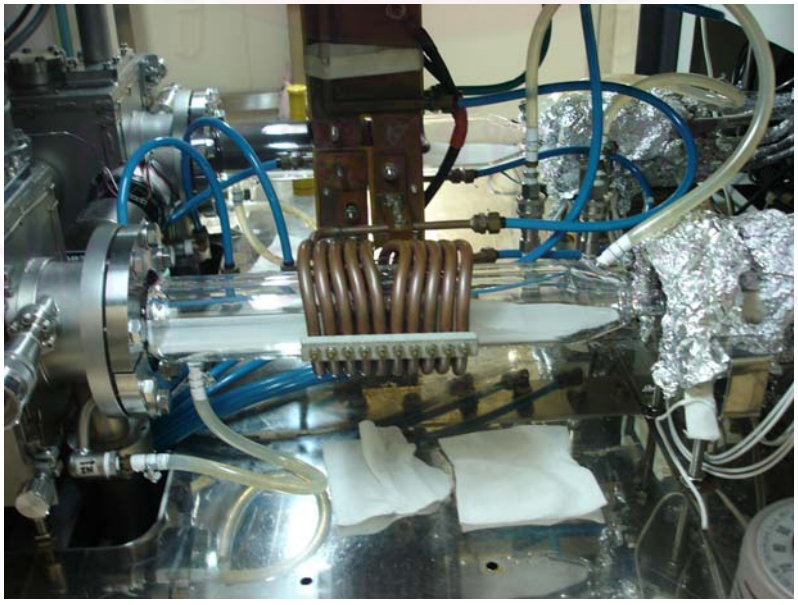

**Fig. 2.1** Horizontal reactor of metal organic vapor phase epitaxy system

metalorganic and/or hydride compounds for group V precursors, will be changed into their gaseous forms before reacting through chemical processes to form compounds. A picture of an MOVPE reactor is shown in Fig. 2.1.

MOVPE growth method is highly complex in both physical and chemical aspects. In this chapter, we describe only the details applied in this work. For more details, we refer to the work of G. B. Stringfellow [28, 29]. During the growth process, precursors will be firstly changed into vapors in the input zone before carried by a carrier gas through a system of tubes to the reactor chamber. The precursors will be transported via an imposed pressure gradient controlled by the pressure adjusting unit. Then, those vapors will enter the mixing zone where they will be mixed to form a homogeneous fluid. This homogeneous fluid will be forced to flow above the substrate, which is heated underneath by a suscepter. Due to a concentration gradient between the fluid layer and the region near the substrate surface, the precursor molecules will travel toward the substrate surface and break through pyrolysis reactions into smaller parts at the surface. Because the concentration of gaseous precursors above the substrate was adjusted to be much higher than its equilibrium value, thermodynamic driving force will drive the gaseous precursors to solidify on the surface. To make solidification, those precursors may react chemically in their gaseous forms and adsorbed on the substrate surface to form the film. Alternatively, they can also be adsorbed directly on the surface in the form of free adatoms before diffuse laterally to find a suitable place on the surface to form a

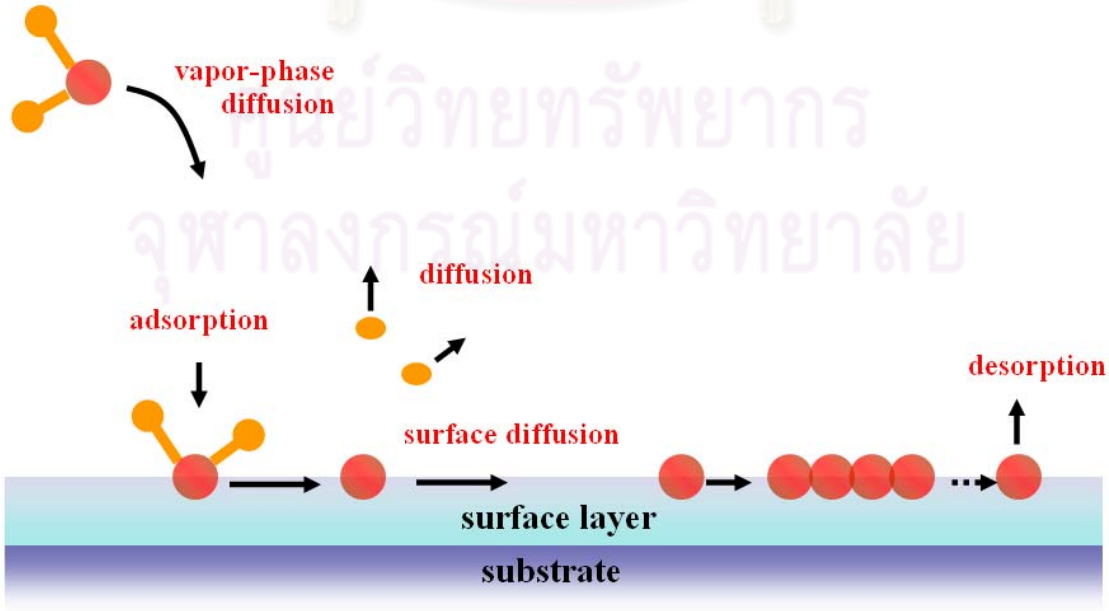


**Fig. 2.2** Processes occurring during the growth under MOVPE process

compound and solidify. Byproducts of those chemical reactions will be pumped out through the exhaust gases treatment system. A schematic diagram of the processes occurring in the surface zone is shown in Fig. 2.2.

SA-MOVPE is a growth technique using MOVPE process. The process is capable of controlling over the area on which the deposition will occur. In this growth technique, dielectric materials such as $SiO_2$ and $SiN_x$ will be firstly grown on the substrate as a mask layer. The area on the mask layer on which the deposition is required will be chemically etched to make an open window. The difference in the crystal structures between dielectric materials (amorphous) and the substrate (single crystal) leads the deposition of the precursors to occur preferably on the exposed substrate surface (window areas).

It was also observed that, under an improper growth condition, polycrystalline can also occur on the masks. The area selectivity in this case is therefore destroyed. Such situation was observed when the partial pressure of the precursors above the masks became higher than a certain critical value or when the growth temperature was too low [30]. In such conditions, the precursors do not have enough energy to move out of the mask area. Consequently, they deposit on the masks. Another situation is when the mask area is too large for the precursors to diffuse out of the mask. Therefore, growth conditions and growth patterns are very sensitive for SA growth.

SA growth usually has higher growth rate than a conventional MOVPE growth process, especially adjacent to mask edges [24, 31]. This is because, in SA growth, the growth is preferred on the exposed areas of the substrate surface. Therefore, an accumulation of precursors occurs above masks. A lateral concentration gradient of the precursors is therefore formed between the masks and the windows. Such lateral gradient was found to cause a growth rate enhancement in the region near masks. Therefore, a growth pattern with wider mask width gives higher growth rate [26]. An extent of the accumulation of precursors was observed to depend on the precursors' diffusion mobility, the precursor species and growth conditions [31 - 33]. In the case of alloys growth, a compositional change was usually found near masks because of the difference in diffusion abilities of different group III precursors [27, 31, 34-36].

## 2.2 Selective area growth of cubic GaN

For SA c-GaN films, different growth features were observed with different mask orientations, different growth temperature, etc. It was found that c-GaN grown on opening stripes aligned along [110] direction on GaAs (001) substrates exhibited to have (111)B sidewalls as shown in Fig.2.3 (a) [37], 2.4 (a) [38], 2.5 (b) [17] and 2.6 (a, c and e) [39]. On the other hand, for [1-10] direction, different growth features were observed with different growth conditions. Wu *et al.* [37] and Sanorpim *et al.* [38] demonstrated c-GaN stripes with (311)A and (111)A sidewalls, as shown in Figs. 2.3(b) and 2.4(b). However, Shen *et al.* [17] reported the stripes with less inclined top surfaces instead of (311)A facets as illustrated in Fig. 2.5(a). In case of c-GaN stripes aligned along the [100] direction, however, as shown in Figs. 2.6 (b, d and f) [39], no distinct facets were observed. Table 2.1 summarizes the growth

**Table 2.1** Growth conditions of previously reported selective area cubic GaN

| Growth Conditions | Wu *et al.* [37] | Sanorpim *et al.* [38] | Shen *et al.* [17] | Sanorpim *et al.* [39] |
|---|---|---|---|---|
| Substrate | GaAs (100) | GaAs (001) | GaAs (001) | GaAs (100) |
| Pressure (Torr) | 160 | 160 | 76 | 160 |
| Source (Ga, N) | TMG, DMHy | TMG, DMHy | TEG, $NH_3$ | TMG, DMHy |
| Mask Material/ Thickness (nm) | $SiN_x$/200 | $SiO_2$/200 | $SiO_2$/70 | $SiO_2$/200 |
| Mask Direction(s) | [011], [01-1] | [110], [1-10] | [110], [1-10] | [011], [001] |
| Fill Factor | 0.8 | 0.5 | 0.3 | 0.5 |
| Buffer layer(s): Material/ Temperature ($^o$C)/ Thickness(nm) | c-GaN/ 575/ 20 | GaAs/ 700/ 100-150<br>c-GaN/ 600/ 20 | GaN/ 700/ 700 | GaAs/ 700/ ~100<br>c-GaN/ 600/ 20 |
| Temperature ($^o$C) | 900 | ~900 | 850 | 900, 930, 960 |
| V/III ratio | Not specified | Not specified | Not specified | 25 |
| Time (min) | 30 | Not specified | 60 | 15 |

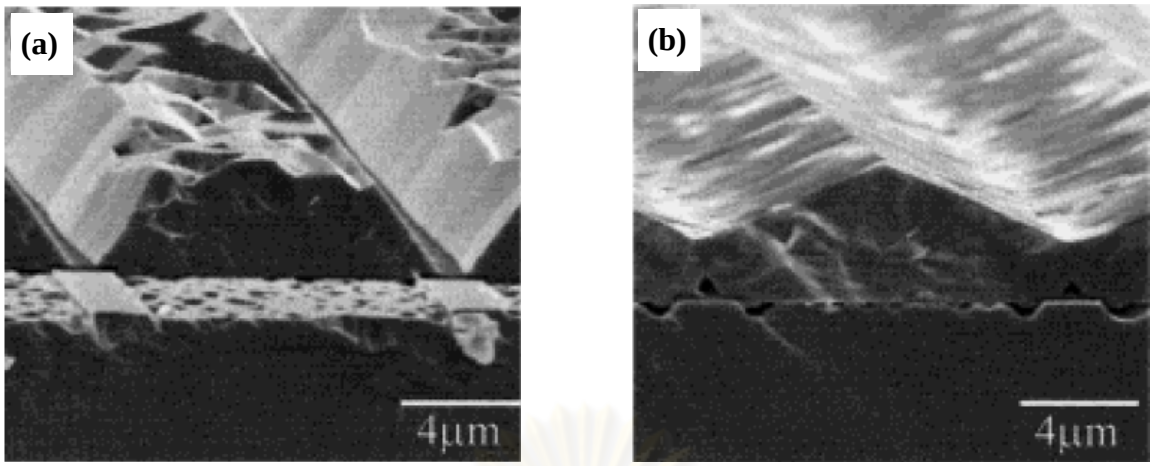


**Fig. 2.3** Cross-sectional SEM images of c-GaN grown on GaAs (001) for 30 min [37]. Stripe orientations are (a) [111] and (b) [1-10] directions.

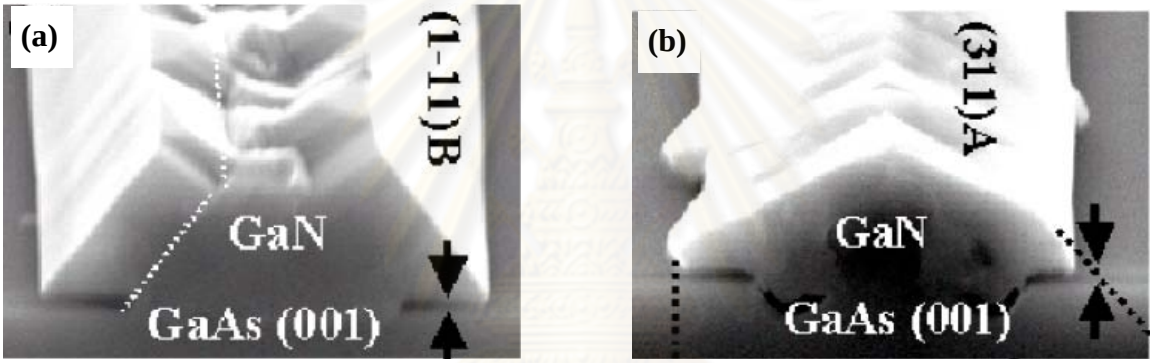


**Fig. 2.4** Cross-sectional SEM images of c-GaN grown on GaAs (001) for 15 min [38]. Stripe orientations are (a) [110] and (b) [1-10] directions.

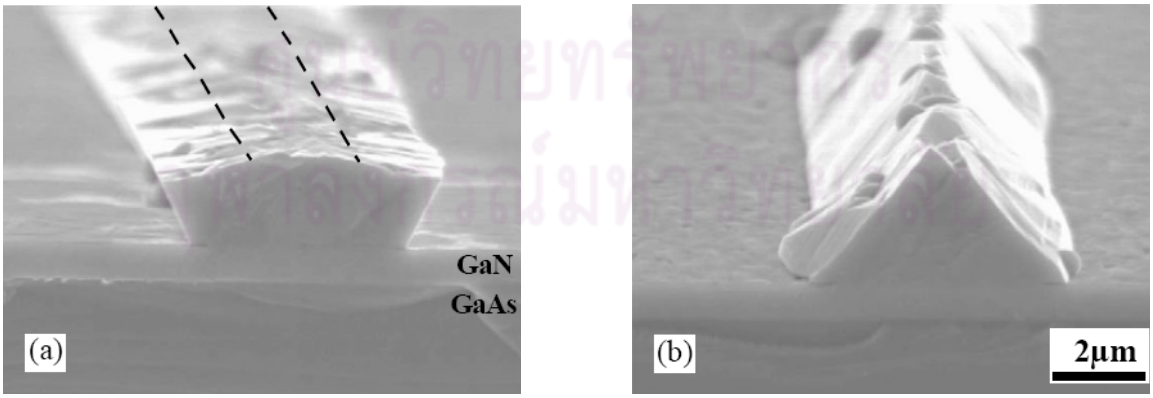


**Fig. 2.5** Cross-sectional SEM images of c-GaN grown on GaAs (001) for 60 min [17]. Stripe orientations are (a) [1-10] and (b) [110] directions.

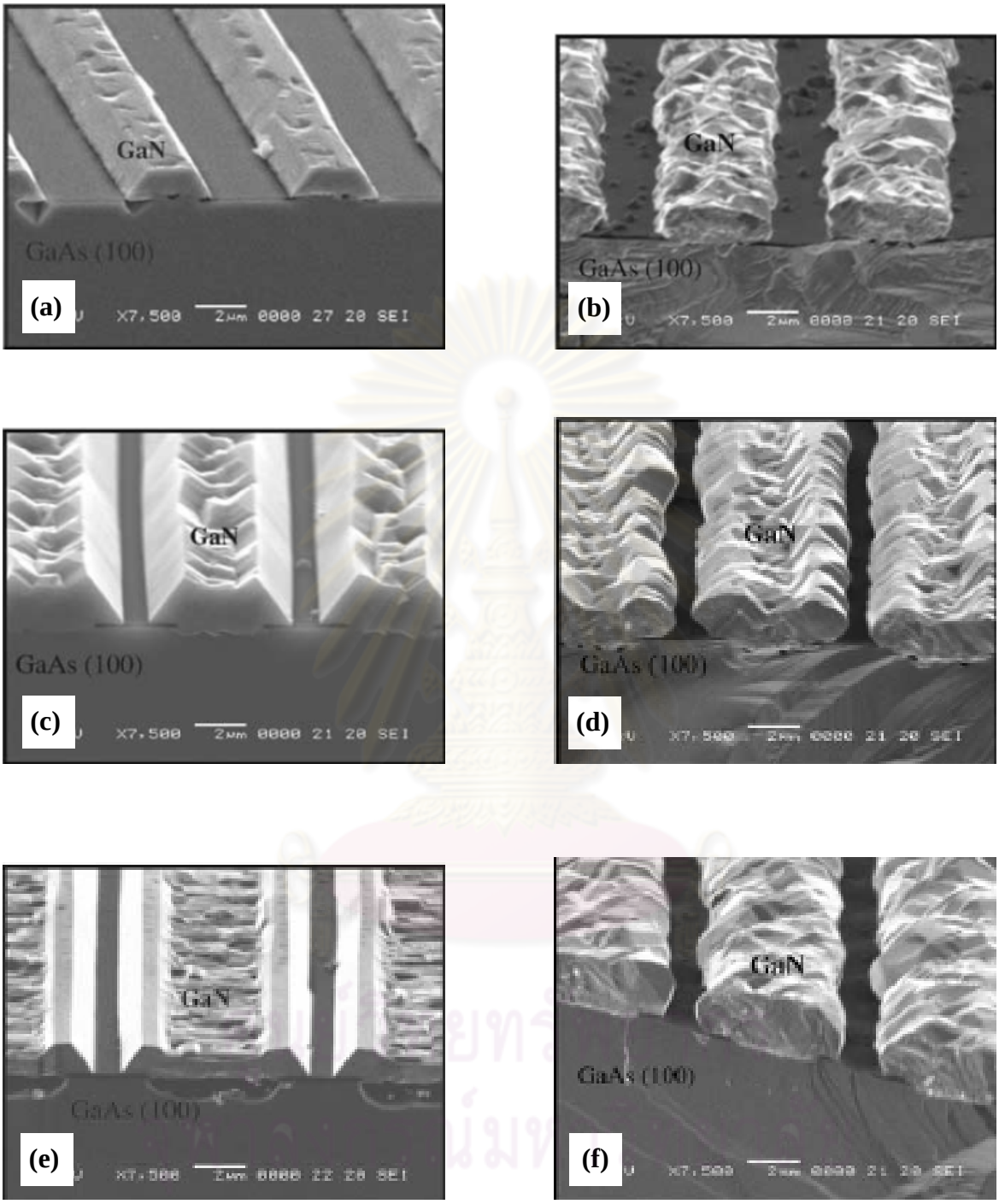


**Fig. 2.6** Cross-sectional SEM images of c-GaN grown on GaAs (001) at growth time of 15 min [39]. (a), (c) and (e): the stripe orientation is [110] and the temperatures are 900, 930 and 960 $^{o}$C, respectively. (b), (d) and (f): the stripe orientation is [100] and the temperatures are 900, 930 and 960 $^{o}$C, respectively.

conditions of c-GaN in each research group. The difference in growth features is still under investigation.

Sanorpim *et al.* [39] reported the effects of growth temperature on growth features of SA c-GaN. The c-GaN stripes along the [110] direction exhibited different facets on the top surfaces at different growth temperatures. The film top surfaces were found to change from inclined (811)B facets to planar (100) facets when the growth temperature was decreased from 960 $^{o}$C to 900 $^{o}$C, as shown in Figs. 2.6 (a, c and e). On the other hand, there is no effect of growth temperature on the (111)B sidewalls of the c-GaN stripes.

## 2.3 Diffusion models

It is known that fluid flow in MOVPE reactors is highly complicated due to the presence of turbulent flow from the nature of viscous fluid and the temperature gradient forming between the flowing fluid layer and the substrate surface. To understand a growth process in SA-MOVPE, therefore, some simplifications have been assumed and various models have been designed. A model will be applicable as long as it can describe a growth aspect of the film within a satisfactory limit. The models we used in this work are also based on several assumptions. The first assumption is that in the growing area, i.e. adjacent to substrate surface, convection and fluid effects are negligible. This type of model, which is known as “a diffusion model”, therefore considers only diffusion processes.

In a diffusion model, the fluid flow adjacent to the substrate surface is usually assumed laminar and a stagnant layer is assumed between the substrate surface and the flowing fluid layer. Within this layer, it is believed that there are two mechanisms taking control over the lateral movement of the precursors, i.e. vapor phase diffusion (VPD) and surface migration (SM). For which processes are more or less dominant, it is distinguished by the distance from masks to the point of nucleation. For the distance larger than 10 μm, VPD was found to dominate [25]. For shorter distance, surface migration process must be taken into account. However, such a result was obtained from a growth experiment where the exposed area (window region) on the substrate surface is much larger than the area covered by dielectric material (mask region). This means that the perturbations from the adjacent patterns can be ignored.

To understand the growth mechanism in SA-MOVPE, we are interested to apply the VPD model [25] and the SM model [40] to study the growth mechanism of SA c-GaN with narrower stripe patterns. Therefore, the models are used as tools to probe the growth phenomena.

These two models are reviewed in section 2.3.1 and 2.3.2, respectively.

### 2.3.1 Vapor phase diffusion model

The vapor phase diffusion (VPD) model was created by Gibbon *et al.* [25] with its benefits in simplicity and versatility. It has been used extensively in SA growth with wide opening windows or high fill factor – defined as "a ratio of opening width to pattern period". Typically, the window widths of several 10 μm were normally used, and the adjustable parameter in VPD model, *D/k*, was found to be about 50 μm or higher. Thus, the perturbation from the adjacent growth patterns can be neglected.

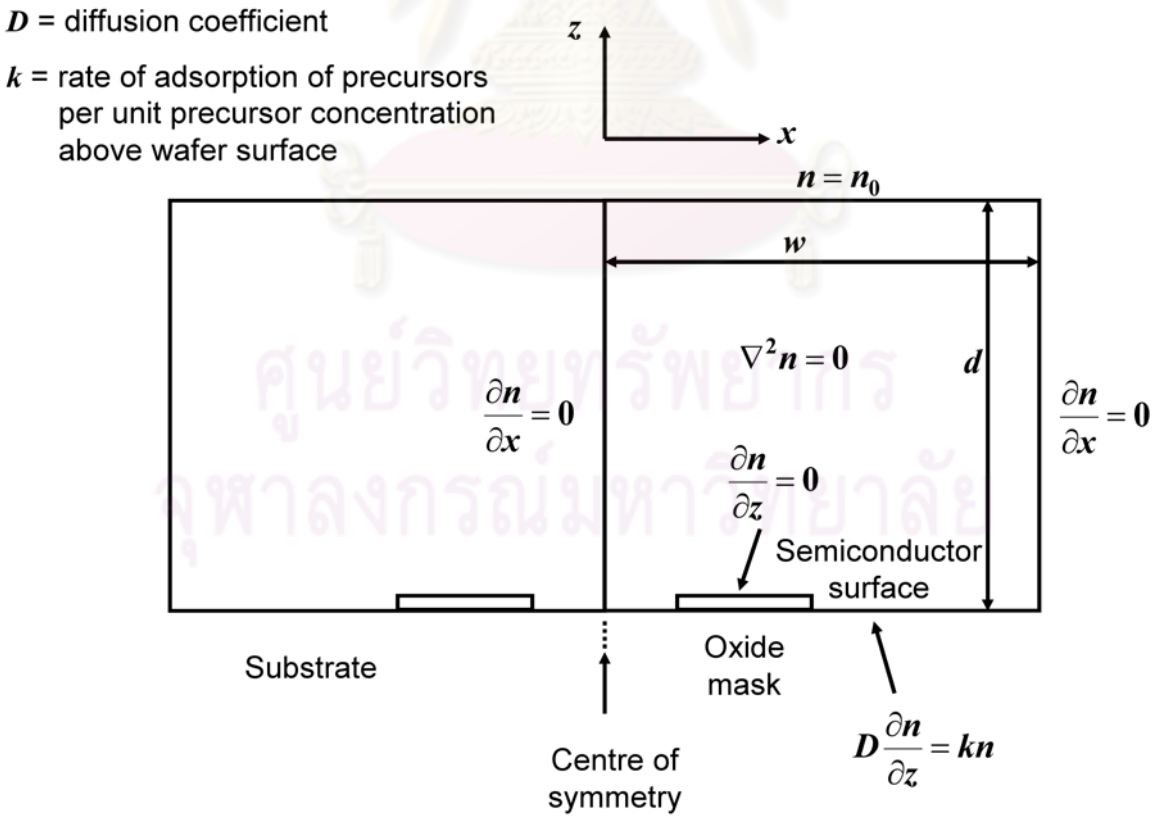


**Fig. 2.7** Diffusion equation and boundary conditions in vapor phase diffusion model [25]

A schematic diagram of VPD model is shown in Fig. 2.7. In this model, a concentration of precursors will be solved from a diffusion model subjected to a set of boundary conditions. The film thickness profile will be deduced directly from the profile of the group III precursor's concentration on the substrate surface. The model is based on several assumptions both from the characteristics of MOVPE process and from those of selective area growth. First, a lateral diffusion of group III precursors on the surface is ignored. This assumption was shown to be applicable for the area of consideration larger than several of 10 μm [25]. Second, no forced convection is presented in the area adjacent to the substrate surface. Therefore, an existence of a stagnant layer, which is a region between the substrate surface and the flowing fluid layer, is assumed. An experimental observation of the formation of the stagnant layer was confirmed by Eversteyn *et al.* [41]. Finally, it is assumed that the stripes have a very long length and are aligned periodically. In an actual situation, the assumption of very long stripes is still applicable if the length of the stripes is longer than the lateral distance that the precursors can move.

Quantitative descriptions of the model are as follows. According to the concentration gradient between the fluid layer and the substrate surface, the precursors will diffuse from the homogeneous fluid layer through the stagnant layer toward the substrate surface. To obtain concentration of precursors on the substrate surface, the concentration in the entire stagnant layer must be obtained. Since there is no force convection in the stagnant layer, the diffusion process obeys the steady state diffusion equation, $\nabla^2 n = 0$, where $n$ is a concentration of the precursors in vapor phase. Then, a set of proper boundary conditions must be selected. Since the upper boundary of the stagnant layer connects to the homogeneous fluid layer, the concentration there can be assumed constant, i.e. independent of position ($x$) and time ($t$). Thus, the upper boundary condition is $n = n_o$. The left and right boundaries are chosen to locate at two symmetric points where the lateral flux of the precursors vanishes, i.e. $D\,\partial n/\partial x = 0$ or $\partial n/\partial x = 0$. In the case of Gibbon *et al.*, such symmetric points were located at the center of two adjacent opening regions. Bottom boundary is located on the surface where regions of mask and window are concerned. Using the fact that the precursors adsorbed on the mask surface will be desorbed back into the vapor, the vertical flux of the precursors onto the mask vanishes, $D\,\partial n/\partial z = 0$ or $\partial n/\partial z = 0$. On the other hand, the precursors are adsorbed with a certain probability before solidify on the window region. For simplicity, the growth

rate is assumed to be linearly dependent on concentration of precursors in vapor phase. Therefore, the vertical flux on window area is equivalent to the deposition rate, $D\,\partial n/\partial z = kn$, where $D$ is the diffusion coefficient of the group-III precursors and $k$ is the rate of adsorption.

However, with several simplifications, some delicate points are not taken into account. For example, any anisotropic properties of the crystal are assumed irrelevant. Diffusion coefficient was also assumed constant and position independent. The latter assumption is equivalent to the assumption of no temperature difference in the stagnant layer. In spite of the fact that the concentration on top of the stagnant layer was assumed position and time independent, the distribution of precursors on the surface is expected to be unperturbed if the height of the stagnant layer is large enough.

The most important parameter in the vapor phase diffusion model is *D/k*. It is known that *D/k*, which has dimension of length, represents lateral diffusion mobility of the precursors. Higher *D/k* gives higher mobility of precursors to diffuse and spread themselves thoroughly above the substrate surface. Effect of *D/k* on the thickness reported by Gibbon *et al.* [25] is shown in Fig. 2.8.

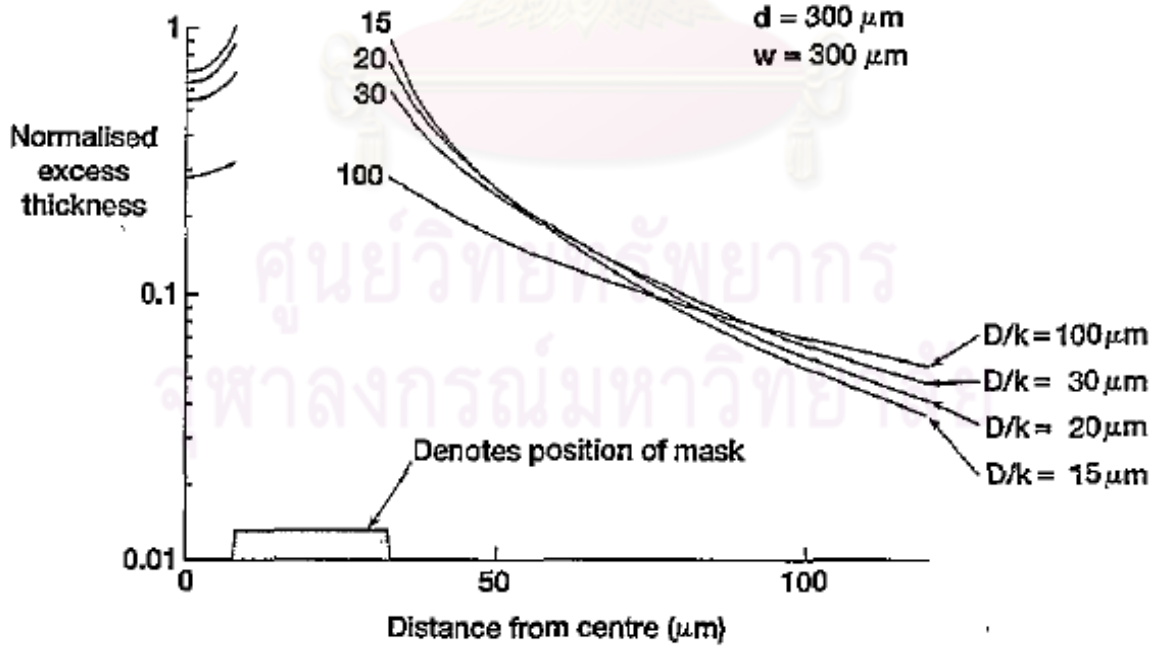


**Fig. 2.8** Calculated profiles of normalized excess thickness at different *D/k*. The profiles show the thickness versus distance from the center of the opening region between two adjacent masks. In this calculation, the pattern period and the height of the stagnant layer were equally set to 300 μm. [25]

Since then, VPD model has been used extensively in the SA growth of many III-V semiconductors. The values of *D/k* observed in those cases are ranging from 50 to 100 μm. However, very recently, Shioda *et al.* [42] applied the model to the case of GaN and found a very interesting result that *D/k* of Ga precursors in the growth of SA GaN was much smaller than those in other III-V semiconductors. The *D/k* was found to be smaller than 10 μm. Therefore, the application of this model to the case of SA growth of c-GaN with narrower stripes (<10 μm) is probable.

## 2.3.2 Surface migration model

A prediction from VPD model was found to successfully explain the film thickness profile in the region located farther than 10 μm from masks [40]. However, the deviation was observed adjacent to the mask edge [40]. To improve the correlation between experimental and the simulation results, Greenspan *et al.* [40] suggested an addition of SM effects of the precursors from no growth (111)B sidewalls, which are usually observed in the case of InP stripes aligned to [110] on (001) substrates. Model's illustration is shown in Fig. 2.9.

As shown in Fig. 2.9, the adatoms absorbed on the no growth (111)B facets can either be desorbed or migrate to (001) top surface. Therefore, in order to calculate the total migration rate of precursors from the (111)B facets, the desorption rate and adsorption rate must be known before hand. The rate of adsorption at one position was obtained by using the assumption of Langmuir [43], i.e. the rate was equivalent to the product of a partial pressure of the precursors above the facets, the number of vacant atomic sites, and the adsorption constant. Similarly, the rate of desorption was the product of occupied atomic sites and the adsorption constant.



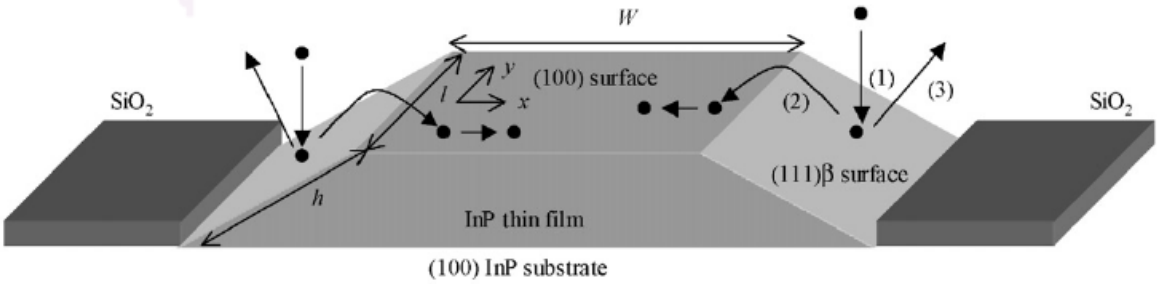


**Fig. 2.9** Diagram of the surface migration model designed by Greenspan *et al*. [40]

Therefore, the conservation of mass leads to Eq. (2.1),

$$k_a p_i(1-\theta) - k_d\theta - N_{so} = 0, \tag{2.1}$$

where $k_a$ is an adsorption constant, $p_i$ is a partial pressure of the precursors, $\theta$ is a percentage of occupied atomic sites, $k_d$ is a desorption constant and $N_{so}$ is a surface migration rate. Moreover, since the concentration of group V precursors in typical growth conditions of III-V semiconductors will be much higher than that of group III, we can assume the percentage of occupied atomic sites of group III precursors to be very small, $\theta_{III} \approx 0$. The migration rate on (111)B facets is, therefore,

$$N_{so} \cong k_a p_i . \tag{2.2}$$

Concerning the case where the inclined length of the sidewall does not exceed the surface migration length of the precursors on the facet, the total number of adatoms migrating from the (111)B facets is the product of the migration rate and the area of the facet. Therefore, considering the cross section of each stripe, the total number of the migrating adatoms to the edges (the point connected the (111)B facet and the top surface) is $n_{so} = hN_{so}$, where $h$ is the inclined length of the (111)B sidewall. The value of $h$ can be calculated from the growth rate ($r_g$) which is obtained from simulation using the VPD model. Therefore, the inclined height $h$ is $h = r_g t \sin^{-1}(55^\circ)$, where $t$ is the growth time, $55^o$ is the inclined angle of (111)B facet when measured from (001) plane. Consequently, the total number of adatoms at the edges is found to be $n_{so} = r_g t k_a p_i \sin^{-1}(55^\circ)$. The concentration of migrating adatoms at a position on (001) surface can then be calculated from time dependent surface diffusion equation with the boundary condition of $n_{so}$. That is,

$$\frac{\partial n_s}{\partial t} = D_s \frac{\partial^2 n_s}{\partial x^2} - \frac{n_s}{\tau}, \tag{2.3}$$

where $D_s$ is a surface diffusion constant and $\tau$ is a mean lifetime of precursor. In the work of Greenspan *et al*. [40], the origin ($x = 0$) was set at the left boundary between (111)B facet and (001) surface, as shown in Fig 2.10. The boundary conditions are given by:

$$n_s(t, x = 0) = r_g k_a p_i (\sin 55^\circ)^{-1} t \equiv At,$$
$$n_s(t, x = W) = At,$$

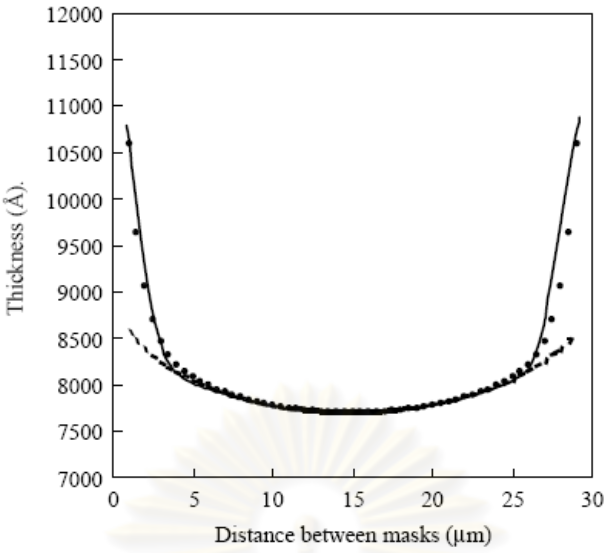


**Fig. 2.10** The thickness profile as a function of the distance from mask. The solid curve is the measured value. The broken and dotted curves are the calculated profile from vapor phase diffusion model and surface migration model, respectively. [40]

and $$n_s(t=0,x)=0. \qquad (2.4)$$

where $W$ is a width of (001) opening surface. For $t>>\tau$, the total number of adatoms was shown to be

$$n_s(t,x)=At\left(e^{-x/L}+e^{-(W-x)/L}\right), \qquad (2.5)$$

where $L^2 = D_s\tau$ is the surface diffusion length of the group III precursors on (001) surface. The film thickness is then calculated from

$$T(t,x)=r_g(x)t+\int_0^t \frac{k_g}{\tau} n_s(x,u)du\ , \qquad (2.6)$$

where, $k_g$ is a molecular volume of InP. Fig. 2.10 shows the results of the SM model compared to the results obtained from the VPD model. It is clearly seen that correlation between experimental and simulated results at the edge regions is remarkably improved.

The SM model was also applied in many cases for both compounds and alloys. For instance, Shioda *et al.* [27] showed an observation of time dependent surface migration. However, all the results were obtained from studies of SA growth with wide stripe patterns (opening width > 50 μm width). Therefore, the surface migration contribution does not have

much effect on the growth rate at the center of the opening window. An observation of the SM contribution was limited to the region near edges. However, we believed that the effects will be much stronger for SA growth with narrower stripe patterns. Therefore, this model is a promising tool to investigate the SA growth of c-GaN with narrow stripe patterns (<10 μm). Investigational results will lead us to find the way to optimize growth conditions in order to control the growth feature of SA c-GaN.

# CHAPTER III
# EXPERIMENT AND MODELING

This chapter is divided into two parts: experiments and modeling. Details of experimental set up such as growth method and growth conditions are given and followed by results and discussion. Then, derivations and modifications of VPD model and SM model are described. Simulation results of these two models will be given and discussed later in chapters 4 and 5.

## 3.1 Experiment

### 3.1.1 Growth of SA c-GaN

In order to understand growth mechanisms of selective area (SA) growth via MOVPE for narrow stripe patterns, we designed to use the pattern, which composed of mask stripe alternating with opening stripe. Width of mask stripe (*M*) was fixed at 4.2 μm in all samples, while width of opening stripes (*W*) of each sample was varied. Each sample will be labeled by its fill factor – defined as the ratio of opening width (*W*) to the pattern period (*W*+*M*). The fill factors used in this work are 0.35, 0.48, 0.58, 0.72 and 1.00. The reference sample is the c-GaN film with no mask (fill factor of 1.00). All samples were grown under the same growth conditions. Details of SA-MOVPE are described as follows.

All the c-GaN samples were grown on pre-patterned GaAs (001) substrates under low-pressure (160 Torr) MOVPE system. To make a pattern on the substrate, 200 nm-thick $SiN_x$ layer was firstly deposited on the GaAs substrates by CVD technique. Then, the SiN layer was etched to make a periodic pattern of opening stripes. Mask width was fixed at 4.2 μm for all samples. The width of opening stripes was varied to adjust the value of fill factor: 0.35, 0.48, 0.58 and 0.72. After patterning the substrate surface, low-temperature GaAs buffer layer (~100 nm thickness) and GaN buffer layer (~20 nm thickness) were grown at 700°C and 600°C, respectively. After the growth of the buffer layers, c-GaN layer was grown at 900$^{o}$C. Trimethylgallium (TMGa), AsH3 and dimethylhydrazine (DMHy) were used as the source materials of Ga, As and N, respectively.

To analyze the pattern effects on the growth feature, scanning electron microscopy (SEM) measurements were performed. Thickness of each sample was examined from SEM images to obtain normalized growth rate, which is defined as the ratio of the thickness at a certain fill factor to the thickness at fill factor 1.00 (no mask condition).

### 3.1.2 Results and discussion

Figure 3.1 shows cross-sectional SEM images of c-GaN stripes with fill factors of (a) 0.35, (b) 0.48, (c) 0.58 and (d) 0.72. It is clearly seen that the selectivity is good for all samples, as no deposition occur on masks. All the samples show cross-section with a trapezoidal shape with very flat (111)B sidewalls and rough (001) top surface. The growth rate enhancement is clearly seen near the edges or at boundary between (001) top surface and (111)B sidewalls.

Normalized growth rate as a function of fill factor is shown in Fig. 3.2. It is evidenced that normalized growth rate of c-GaN stripes with smaller fill factor is remarkably higher than

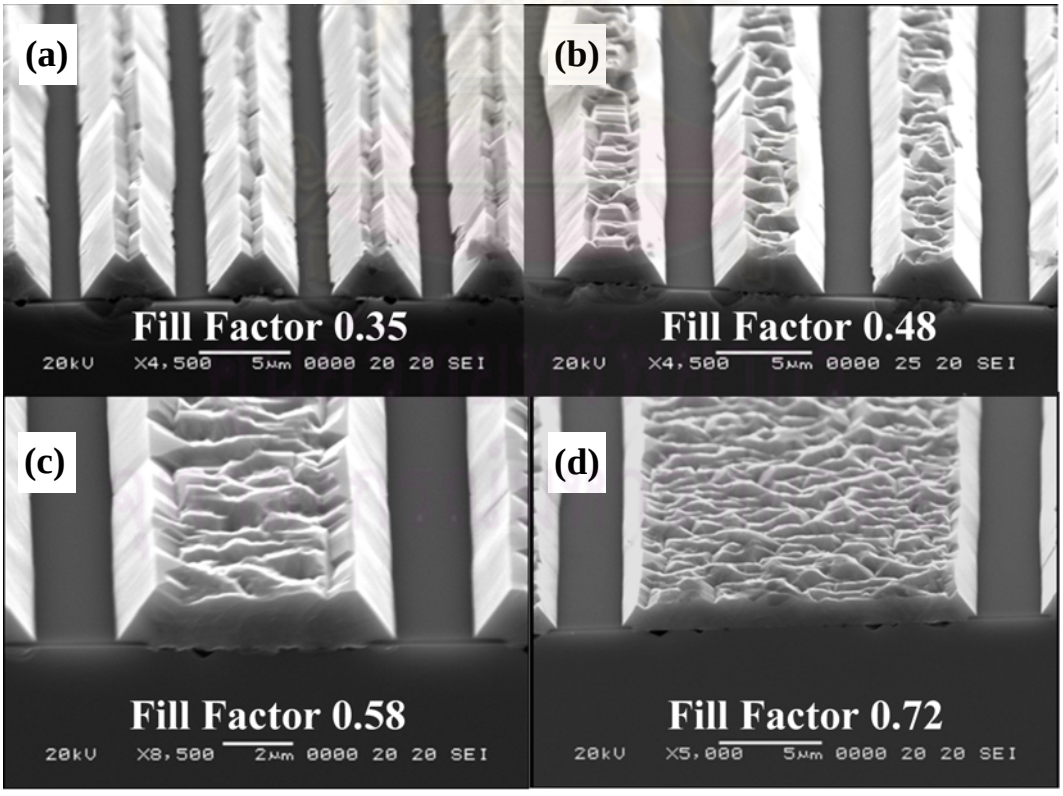


**Fig. 3.1** Bird eye view SEM images of SA c-GaN on GaAs (001) substrates with stripe pattern along [110] direction and fill factor of (a) 0.35, (b) 0.48, (c) 0.58 and (d) 0.72.

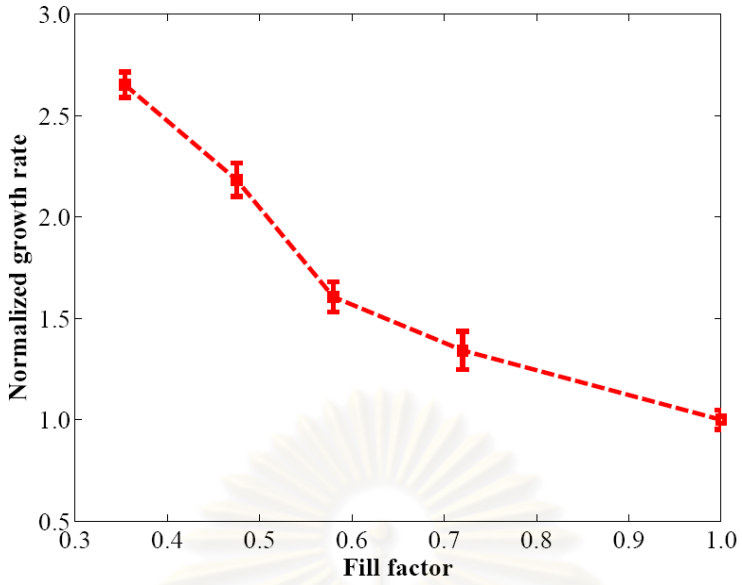


**Fig. 3.2** Normalized growth rate of c-GaN stripes grown on a GaAs (001) substrate patterned lengthwise along [110] direction as a function of fill factor

that of c-GaN stripes with greater fill factor. Compared to c-GaN film with no mask, the growth rate of SA c-GaN stripes is enhanced, indicating growth rate enhancement due to SA growth technique.

Figure 3.3 shows cross-sectional transmission electron microscopy (TEM) images of a c-GaN stripe grown at the same growth condition with $SiO_2$ mask material, which were

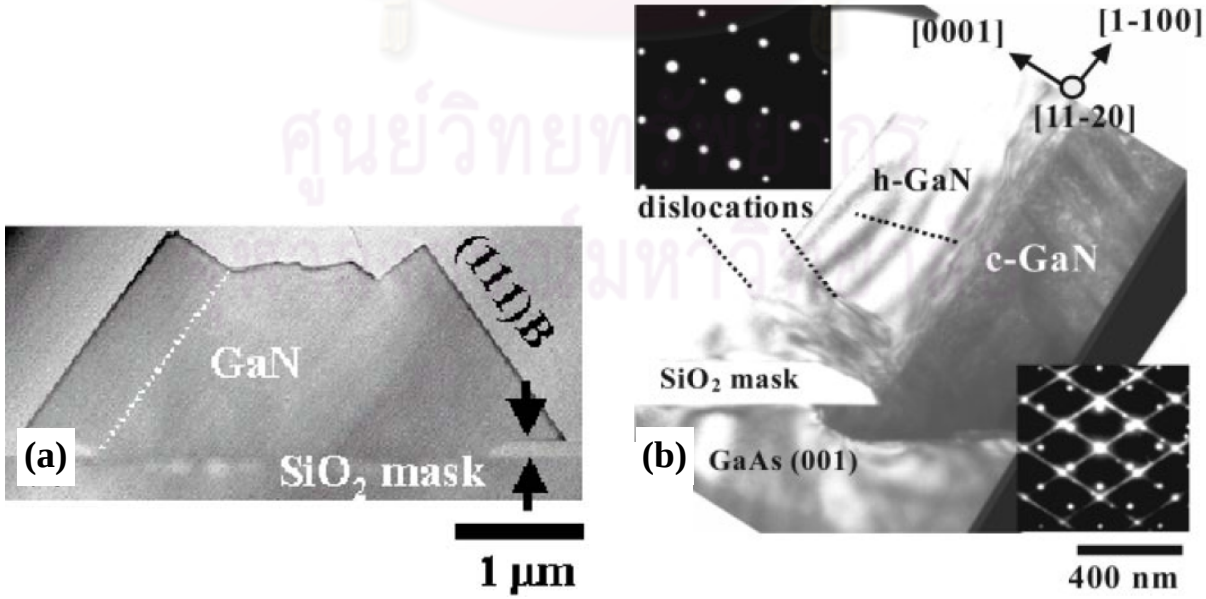


**Fig. 3.3 (a)** Low-magnification and **(b)** higher magnification transmission electron microscopy (TEM) images of GaN stripes with fill factor of 0.5 and mask width of 3 µm. The stripe is oriented along the [110] direction. [38]

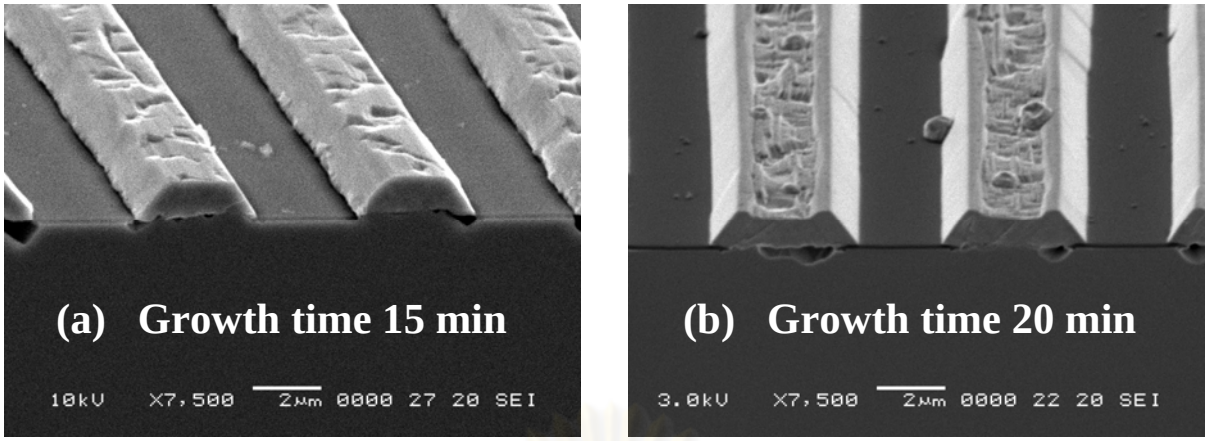


**Fig. 3.4** Bird eye view SEM images of c-GaN stripes on [110]-patterned GaAs (001) substrates grown at 880 $^{o}$C with growth times of (a) 15 min and (b) 20 min.

reported by Sanorpim *et al.* [38]. It was found that GaN crystallized in cubic structure only in the region above the opening surface of the substrate. On the other hand, pure hexagonal structure of GaN was observed to be laterally overgrown on the mask regions.

### 3.1.3 Growth features of c-GaN stripes as time proceeds

Interestingly, GaN was found to grow only on the opening region without any lateral overgrowth until a certain growth time. Figure 3.4 shows SEM images of c-GaN stripes grown at 880$^{o}$C for (a) 15 and (b) 20 min oriented along the [110] direction. Growth conditions of these films are identical. As seen in Fig. 3.4 (a), deposition of c-GaN occurred only above the opening region. On the other hand, lateral overgrowth later occurred for the film with longer growth time (20 min) as shown in Fig. 3.4 (b).

## 3.2 Modeling

### 3.2.1 Vapor phase diffusion model

Diffusion equation and boundary conditions appearing in the vapor phase diffusion model being used in our analysis are illustrated in Fig. 3.5. The area above the substrate surface is assumed stagnant, i.e. forced convection is not concerned. Thus, according to the conservation of mass, group III precursor (Ga) concentration ($u$) in the area of the stagnant layer satisfies a steady state diffusion equation with no source term, $\Delta u = 0$. Above the stagnant layer, which is the zone under the influence of fluid flow, the flowing substances are assumed well mixed and homogeneous. The Ga concentration above the stagnant layer is then

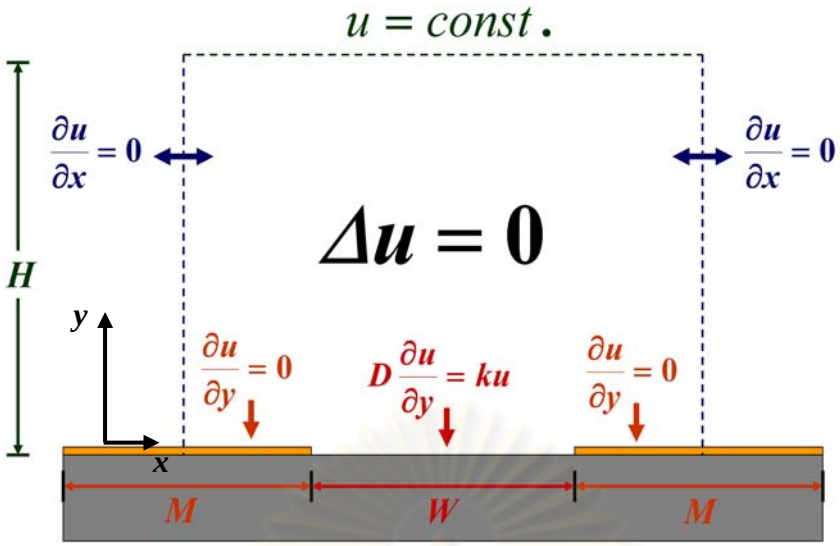


**Fig. 3.5** Diffusion equation and boundary conditions in vapor phase diffusion model

assumed constant, time and position independent. The left and right boundaries are chosen to be located at the center of two adjacent mask stripes and imposed the condition of no lateral flux of Ga precursors due to their symmetry, $\partial u/\partial x = 0$. The bottom boundary is located on the surface where two different types of area must be concerned, i.e. the opening region and the region covered with mask. On the opening region, the condition of continuous flux is applied in conjunction with Langmuir isotherm [43] and Fick's law. This results in $D\partial u/\partial y = ku$ , where $D$ and $k$ are diffusion coefficient and deposition rate constant, respectively. According to the growth results, no growth on the masks is assumed. Therefore, the condition $\partial u/\partial y = 0$ was applied on the mask area.

In order to investigate effects of VPD process on c-GaN narrow stripes, VPD model was translated into a computational program using MATLAB. To solve the diffusion equation with the boundary conditions, a finite different method was applied. The area in the stagnant layer was considered as a rectangular grid system. The grid spacing in the vertical and horizontal directions was set independently. At all grid points, the diffusion equation was changed to a finite difference equation. The central difference approximation was applied at all the points located inside the boundary. At the points on the left, right and bottom boundaries, the equation was adapted by using a forward or backward difference approximation in conjunction with the imposed boundary conditions. All the points at the topmost of the rectangular domain were equally fixed to a certain constant at all time.

Concerning the nature of diffusion process, the precursor concentration will vary until the saturation occurs. Therefore, the program was set to cease when the percent of concentration difference (between the present and the previous round) at the center of the opening region on the substrate surface is less than a specific value (0.5%). To get rid of an unnecessary retardation resulted from too many calculations and to avoid an unwanted stop resulted from a too small variation of the concentration which always happens during the initial stage of the running, the calculation of the percent of difference was set to execute only when the program is running through a set of specific round numbers. In this work, the calculation was set to perform when the program reaches a round number which is an integral multiple of 10,000 i.e. the round number 10,000, 20,000, 30,000, etc.

## 3.2.2 Surface migration model

Surface migration process was shown to have noticeable effects in the area within 10 μm distance from no growth area [25]. Therefore, in the case where the opening width is comparable to 10 μm, surface migration effects should be concerned. According to the experimental results, Figs. 3.3 and 3.4, we believed that the c-GaN stripes possibly grew under two-step growth process as shown in Fig. 3.6. In the first step, c-GaN grows directly on the opening region of the substrate surface with a trapezoid shape with (111)B sidewalls. In this stage, the growth rate of (111)B facets was assumed to be negligibly low until the length of the facet exceeded the surface diffusion length of the Ga precursors [33]. The second step, namely lateral overgrowth, will begin after the length of the (111)B facets exceeds the

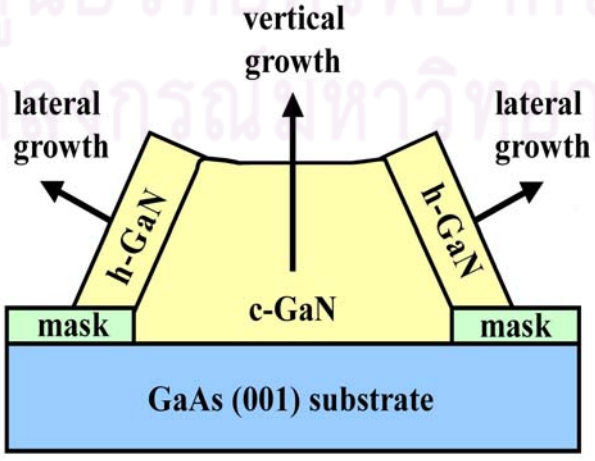


**Fig. 3.6** Schematic diagram of two-step growth process [38]

diffusion length of the Ga precursors, resulting in both lateral and vertical growth. Without disturbance, this stage would continue until coalescence.

The experimental supports of the two-step growth model are as follows. As shown in Fig. 3.1, (111)B facets appear apparently as sidewalls of the c-GaN stripes. Moreover, according to TEM results of SA c-GaN films grown at the same growth conditions shown in Figs. 3.3 (a) and (b), the films have cubic structure only in the trapezoidal region (region I, the first step growth) above the opening substrate surface, which was bounded by (111)B sidewalls. For the lateral growth region (region II, the second step growth) which started from (111)B facets, GaN crystallizes in hexagonal phase. This difference in the crystal structures suggested two different growth processes. To analyze the growth features of c-GaN stripes above the opening regions, we therefore ignored the lateral growth.

According to two-step growth model, during the first step, the surface migration model of Greenspan *et al.* [40] can be applied. The schematic diagram of the first-step growth is shown in Fig. 3.7. In this work, the origin of *x* axis on (001) plane was located at the center of the opening region. The reason of changing the position from the model used in Greenspan *et al.*'s work is to enable the upcoming solution to be applied to a more general case, i.e. the case where the decreasing in the width of the opening region is concerned. Consequently, the surface diffusion equation is

$$\frac{\partial n}{\partial t} = D_s \frac{\partial^2 n}{\partial x^2} - \frac{n}{\tau}. \qquad (3.1)$$

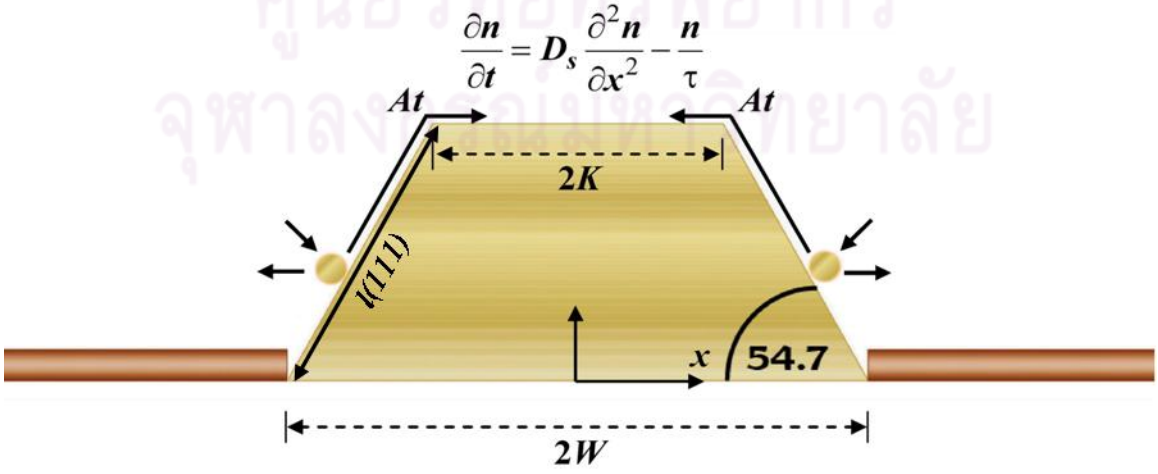


**Fig. 3.7** Schematic diagram of the first-step growth process in which no lateral overgrowth is involved

in conjunction with

$$n(t, x = \pm K) = r_g k_a p_i \left(\sin 54.7^\circ\right)^{-1} t \equiv At, \tag{3.2}$$

$$n(t = 0, x) = 0, \tag{3.3}$$

where $n$ is a concentration of group III precursors on (001) surface, $x$ is a position from the centre of the open window, $t$ is a growth time, $D_s$ is a surface diffusion constant of group III precursors on (001) surface, $\tau$ is an average lifetime of group III precursors on (001) surface, $r_g$ is the growth rate derived from VPD model, $k_a$ is an adsorption constant of group III precursors on (111)B facet, $p_i$ is a partial pressure of group III precursors on (111)B facet and $K$ is a half of the opening width. To solve Eq. (3.1) with boundary conditions (3.2)-(3.3), let us consider a function in a form of

$$u(t, x) = e^{t/\tau} n(t, x). \tag{3.4}$$

Substituting Eq. (3.4) into Eqs. (3.1)-(3.3), we obtain

$$\frac{\partial u}{\partial t} = D_s \frac{\partial^2 u}{\partial x^2}, \tag{3.5}$$

with

$$u(t, x = \pm K) = e^{t/\tau} At, \tag{3.6}$$

$$u(t = 0, x) = 0. \tag{3.7}$$

Then, let

$$v(t, x) = u(t, x) - e^{t/\tau} At. \tag{3.8}$$

Substituting Eq. (3.8) into Eqs. (3.5)-(3.7), we obtain

$$\frac{\partial v}{\partial t} = D_s \frac{\partial^2 v}{\partial x^2} - \left(1 + \frac{t}{\tau}\right) A e^{t/\tau}, \tag{3.9}$$

with

$$v(t, x = \pm K) = 0, \tag{3.10}$$

$$v(t = 0, x) = 0. \tag{3.11}$$

To solve Eq. (3.9) with boundary conditions (3.10)-(3.11), we note that the solution of these equations must be symmetric around the origin, i.e. the solution must be an even function. Therefore, we expect the solution to be expandable by cosine Fourier series. Therefore, we try the solution in the following form:

$$v(t,x)=\sum_{n=1}^{\infty}C_n(t)\cos(\lambda_n x). \tag{3.12}$$

The boundary condition (3.10) suggests

$$\lambda_n K=\frac{\pi}{2}(2n-1). \tag{3.13}$$

Expand $Ae^{t/\tau}\left(1+\frac{t}{\tau}\right)$ by

$$Ae^{t/\tau}\left(1+\frac{t}{\tau}\right)=\sum_{n=1}^{\infty}S_n(t)\cos(\lambda_n x). \tag{3.14}$$

The coefficient $S_n(t)$ can be obtained from the relation,

$$\begin{aligned} S_n(t) &= Ae^{t/\tau}\left(1+\frac{t}{\tau}\right)\frac{\int_{-K}^{K}\cos(\lambda_n x)dx}{\int_{-K}^{K}\cos^2(\lambda_n x)dx} \\ &= Ae^{t/\tau}\left(1+\frac{t}{\tau}\right)\left(\frac{2\cdot(-1)^{n+1}}{K\lambda_n}\right). \end{aligned} \tag{3.15}$$

Substitute Eqs. (3.12), (3.14) and (3.15) into Eq. (3.9). We obtain

$$\sum_{n=1}^{\infty}\left[\frac{dC_n}{dt}+D_s\lambda_n{}^2C_n+S_n\right]\cos(\lambda_n x)=0, \tag{3.16}$$

which implies that the coefficients of $\cos(\lambda_n x)$ vanish for all $n$.

We solved Eq. (3.16) by using the formula:

$$\begin{aligned} C_n &= -\left(\frac{1}{e^{\int D_s\lambda_n{}^2dt}}\right)\left(\int S_n\cdot e^{\int D_s\lambda_n{}^2dt'}dt\right)+c_1e^{-\int D_s\lambda_n{}^2dt} \\ &= \left(\frac{1}{e^{\int D_s\lambda_n{}^2dt}}\right)\left(\frac{2(-1)^n A}{\lambda_n K}\right)\left(\int e^{\left(D_s\lambda_n{}^2+\frac{1}{\tau}\right)\cdot t}\left(1+\frac{t}{\tau}\right)dt\right)+c_1e^{-D_s\lambda_n{}^2t}, \end{aligned} \tag{3.17}$$

where $c_1$ is a constant of integration.

Since

$$\int e^{\left(D_s\lambda_n{}^2+\frac{1}{\tau}\right)\cdot t}\,dt=\frac{e^{\left(D_s\lambda_n{}^2+\frac{1}{\tau}\right)\cdot t}}{D_s\lambda_n{}^2+\frac{1}{\tau}}, \tag{3.18}$$

and

$$\frac{1}{\tau}\int te^{\left(D_s\lambda_n{}^2+\frac{1}{\tau}\right)\cdot t}\,dt=\frac{1}{\tau}\left[\frac{te^{\left(D_s\lambda_n{}^2+\frac{1}{\tau}\right)\cdot t}}{D_s\lambda_n{}^2+\frac{1}{\tau}}-\frac{e^{\left(D_s\lambda_n{}^2+\frac{1}{\tau}\right)\cdot t}}{\left(D_s\lambda_n{}^2+\frac{1}{\tau}\right)^2}\right]. \tag{3.19}$$

Therefore,

$$C_n=\frac{2\cdot(-1)^n Ae^{t/\tau}}{K\lambda_n}\left(\frac{1}{D_s\lambda_n{}^2+\frac{1}{\tau}}\right)\left(1+\frac{t}{\tau}-\frac{1}{\left(D_s\lambda_n{}^2+\frac{1}{\tau}\right)\cdot\tau}\right)+c_1e^{-D_s\lambda_n{}^2t}. \tag{3.20}$$

Using Eq. (3.11), we obtain

$$c_1=-\frac{2\cdot(-1)^n A}{K\lambda_n}\left(\frac{1}{D_s\lambda_n{}^2+\frac{1}{\tau}}\right)\left(1-\frac{1}{\left(D_s\lambda_n{}^2+\frac{1}{\tau}\right)\cdot\tau}\right). \tag{3.21}$$

Substituting Eq. (3.21) into Eq. (3.20), we obtain

$$C_n=\frac{2\cdot(-1)^n A}{K\lambda_n}\left(\frac{1}{D_s\lambda_n{}^2+\frac{1}{\tau}}\right)\left(e^{t/\tau}\left\{1+\frac{t}{\tau}-\frac{1}{\left(D_s\lambda_n{}^2+\frac{1}{\tau}\right)\cdot\tau}\right\}-e^{-D_s\lambda_n{}^2t}\left\{1-\frac{1}{\left(D_s\lambda_n{}^2+\frac{1}{\tau}\right)\cdot\tau}\right\}\right),$$

$$=\frac{2\cdot(-1)^n A}{K\lambda_n}\left(\frac{1}{D_s\lambda_n{}^2+\frac{1}{\tau}}\right)\left(e^{t/\tau}\left\{1+\frac{t}{\tau}-\frac{1}{\left(D_s\lambda_n{}^2+\frac{1}{\tau}\right)\cdot\tau}\right\}-e^{-\left(D_s\lambda_n{}^2\tau\right)\frac{t}{\tau}}\left\{1-\frac{1}{\left(D_s\lambda_n{}^2+\frac{1}{\tau}\right)\cdot\tau}\right\}\right). \tag{3.22}$$

Using the approximation that $t/\tau >> 1$, we therefore obtain

$$C_n \cong \frac{2\cdot(-1)^n Ae^{t/\tau}}{K\lambda_n}\left(\frac{1}{D_s{\lambda_n}^2+\frac{1}{\tau}}\right)\left(\frac{t}{\tau}-\frac{1}{\left(D_s{\lambda_n}^2+\frac{1}{\tau}\right)\cdot\tau}\right). \tag{3.23}$$

We define $L^2 = D_s\tau$ as the surface migration length of the precursor on the (001) surface. Therefore,

$$C_n \cong \frac{2\cdot(-1)^n Ae^{t/\tau}}{K\lambda_n}\left(\frac{\tau}{L^2{\lambda_n}^2+1}\right)\left(\frac{t}{\tau}-\frac{1}{L^2{\lambda_n}^2+1}\right). \tag{3.24}$$

Substitute Eq. (3.24) into Eqs. (3.12), (3.8) and (3.4). We obtain

$$n(t,x) = At + \sum_{n=1}^{\infty}\frac{2\cdot(-1)^n A}{K\lambda_n}\left(\frac{\tau}{L^2{\lambda_n}^2+1}\right)\left(\frac{t}{\tau}-\frac{1}{L^2{\lambda_n}^2+1}\right)cos(\lambda_n x)$$

$$\cong At + At\sum_{n=1}^{\infty}\frac{2\cdot(-1)^n}{K\lambda_n}\left(\frac{1}{L^2{\lambda_n}^2+1}\right)cos(\lambda_n x) \tag{3.25}$$

where we have used $\frac{t}{\tau} >> \frac{1}{L^2{\lambda_n}^2+1}$.

In order to generate a function from the series appearing in Eq. (3.25), we consider cosine Fourier series of a hyperbolic cosine function, $cosh(ax) = \sum_{n=1}^{\infty} A_n cos(\lambda_n x)$ . Its coefficients are

$$A_n = \frac{\int_{-K}^{K} cosh(ax)cos(\lambda_n x)dx}{\int_{-K}^{K} cos^2(\lambda_n x)dx}$$

$$= \frac{1}{K}\left[\frac{1}{a^2+{\lambda_n}^2}\left(\lambda_n sin(\lambda_n x)cosh(ax)+a\,cos(\lambda_n x)sinh(ax)\right)\right]_{x=-K}^{x=K}$$

$$= \frac{1}{K}\left(\frac{1}{a^2+{\lambda_n}^2}\right)\cdot 2\lambda_n(-1)^{n+1}cosh(aK) \tag{3.26}$$

Therefore,

$$cosh(ax) = \sum_{n=1}^{\infty}\frac{1}{K}\left(\frac{1}{a^2+{\lambda_n}^2}\right)\cdot 2\lambda_n(-1)^{n+1}cosh(aK)cos(\lambda_n x). \tag{3.27}$$

Integrating Eq. (3.27) twice, we obtain

$$\frac{\cosh(ax)}{a^2} + c_2 x + c_3 = \sum_{n=1}^{\infty} \frac{1}{K}\left(\frac{1}{a^2 + \lambda_n{}^2}\right) \cdot 2\lambda_n (-1)^{n+1} \cosh(aK)\left(\frac{\cos(\lambda_n x)}{\lambda_n{}^2}\right)$$

$$= \left(\frac{\cosh(aK)}{a^2}\right)\left[\sum_{n=1}^{\infty} \frac{1}{K}\left(\frac{1}{1+\left(\frac{\lambda_n}{a}\right)^2}\right) \cdot 2(-1)^{n+1} \cosh(aK)\left(\frac{\cos(\lambda_n x)}{\lambda_n}\right)\right], \tag{3.28}$$

where $c_2$ and $c_3$ are constants of integration. Since $\cos(\pm\lambda_n K) = 0$ for all $n$, we obtain $c_2 = 0$ and $c_3 = -\frac{\cosh(aK)}{a^2}$. Comparing Eq. (3.28) and Eq. (3.25), we obtain

$$\begin{aligned} n(t,x) &\cong At + At\left[\frac{\cosh(x/L) - \cosh(K/L)}{\cosh(K/L)}\right]. \\ &= At\frac{\cosh(x/L)}{\cosh(K/L)}. \end{aligned} \tag{3.29}$$

where $At = r_g t\left(\sin 54.7^\circ\right)^{-1} k_a p_i = k_a p_i l(111)$. Alternatively, Eq. (3.29) can be rewritten as

$$n(t,x) \cong k_a p_i l(111)\frac{\cosh(x/L)}{\cosh(K/L)}. \tag{3.30}$$

That is, the diffusion equation (3.1) with boundary conditions (3.2) and (3.3) predicts the precursor concentration profile on the surface to be a linearly function of growth time. Eq. (3.29) also leads the thickness to be composed of two terms as shown in Eq. (3.31).

$$\begin{aligned} T(t,x) &\cong r_g(x)t + \int_0^t \frac{k_g}{\tau} n_s(x,u)du \\ &= r_g(x)t + \left(\frac{k_g k_a p_i \left(\sin 54.7^\circ\right)^{-1}}{2\tau} \cdot \frac{\cosh(x/L)}{\cosh(K/L)}\right) \cdot r_g(x)t^2 \\ &= r_g(x)t + \frac{k_g}{2\tau} n(t,x)t, \end{aligned} \tag{3.31}$$

where $k_g$ is molecular volume of the film. The first term on the right hand side of the thickness equation (3.31) resulted from VPD process, while the second term represents the surface contribution. To obtain the growth rate of the film, consider the first derivative of Eq. (3.31).

This indicates that surface contribution effects lead the growth rate to depend linearly on time instead of being time independent as observed in the case of VPD model.

It should be note that during the derivation, we have calculated $l(111)$ using the growth rate calculated from VPD model, i.e. $l(111)$ was assumed to grow with time-independent growth rate. However, Eq. (3.31) suggested that time dependent aspects exist in this case. To improve, therefore, $l(111)$ was modified to be derived from the thickness equation (3.31). Therefore, Eqs. (3.1) to (3.3) will change to be

$$\frac{\partial n}{\partial t} = D_s \frac{\partial^2 n}{\partial x^2} - \frac{n}{\tau} \tag{3.32}$$

with

$$\begin{aligned} n(t, x = \pm K) &= k_a p_i l(111)_{VPD+Surf} \\ &= k_a p_i \left(\sin 54.7^\circ\right)^{-1} \cdot T(t, x = 0) \\ &= k_a p_i \left(\sin 54.7^\circ\right)^{-1} \left( r_g t + \frac{k_g r_g k_a p_i \left(\sin 54.7^\circ\right)^{-1}}{2\tau} t^2 \right) \equiv At + Bt^2, \end{aligned} \tag{3.33}$$

$$n(t = 0, x) = 0, \tag{3.34}$$

where $A \equiv k_a p_i r_g \left(\sin 54.7^\circ\right)^{-1}$ and $B \equiv \frac{k_g k_a p_i \left(\sin 54.7^\circ\right)^{-1}}{2\tau} A$.

Using

$$u(t, x) = e^{t/\tau} n(t, x), \tag{3.35}$$

and substituting Eq. (3.35) into Eqs. (3.32)-(3.34), we obtain

$$\frac{\partial u}{\partial t} = D_s \frac{\partial^2 u}{\partial x^2} \tag{3.36}$$

with

$$u(t, x = \pm K) = e^{t/\tau} \left(At + Bt^2\right), \tag{3.37}$$

$$u(t = 0, x) = 0. \tag{3.38}$$

Then, let

$$v(t,x) = u(t,x) - e^{t/\tau}\left(At + Bt^2\right). \tag{3.39}$$

Substituting Eq. (3.39) into Eqs. (3.36)-(3.38), we obtain

$$\frac{\partial v}{\partial t} = D_s \frac{\partial^2 v}{\partial x^2} - \left(1 + \frac{t}{\tau}\right) A e^{t/\tau} - \left(2t + \frac{t^2}{\tau}\right) B e^{t/\tau}, \tag{3.40}$$

with

$$v(t, x = \pm K) = 0, \tag{3.41}$$

$$v(t = 0, x) = 0. \tag{3.42}$$

To solve Eq. (3.40) with boundary conditions (3.41) - (3.42), we try the solution in the form,

$$v(t,x) = \sum_{n=1}^{\infty} C_n(t) \cos(\lambda_n x). \tag{3.43}$$

which was suggested by the symmetry of the equations around the point ($x$ = 0).

The boundary condition (3.41) suggests

$$\lambda_n K = \frac{\pi}{2}(2n-1). \tag{3.44}$$

Expand $\left(2t - \frac{t^2}{\tau}\right) B e^{t/\tau}$ by

$$B e^{t/\tau}\left(2t + \frac{t^2}{\tau}\right) = \sum_{n=1}^{\infty} Q_n(t) \cos(\lambda_n x). \tag{3.45}$$

We obtain

$$Q_n(t) = \mathrm{B} e^{t/\tau}\left(2t + \frac{t^2}{\tau}\right)\left(\frac{2 \cdot (-1)^{n+1}}{K\lambda_n}\right). \tag{3.46}$$

Substitute Eqs. (3.43), (3.14), (3.15), (3.45) and (3.46) into Eq. (3.40). We obtain

$$\sum_{n=1}^{\infty}\left[\frac{dC_n}{dt} + D_s \lambda_n{}^2 C_n + S_n + Q_n\right] \cos(\lambda_n x) = 0. \tag{3.47}$$

Solve for $C_n$ by using the formula:

$$C_n = -\left(\frac{1}{e^{\int D_s\lambda_n{}^2 dt}}\right)\left(\int S_n \cdot e^{\int D_s\lambda_n{}^2 dt'} dt\right) - \left(\frac{1}{e^{\int D_s\lambda_n{}^2 dt}}\right)\left(\int Q_n \cdot e^{\int D_s\lambda_n{}^2 dt'} dt\right) + c_1 e^{-\int D_s\lambda_n{}^2 dt}$$

$$= \left(\frac{1}{e^{\int D_s\lambda_n{}^2 dt}}\right)\left(\frac{2(-1)^n A}{\lambda_n K}\right)\left(\int e^{\left(D_s\lambda_n{}^2+\frac{1}{\tau}\right)\cdot t}\left(1+\frac{t}{\tau}\right)dt\right)$$

$$+ \left(\frac{1}{e^{\int D_s\lambda_n{}^2 dt}}\right)\left(\frac{2(-1)^n B}{\lambda_n K}\right)\left(\int e^{\left(D_s\lambda_n{}^2+\frac{1}{\tau}\right)\cdot t}\left(2t+\frac{t^2}{\tau}\right)dt\right) + c_1 e^{-D_s\lambda_n{}^2 t}, \quad (3.48)$$

where $c_1$ is a constant of integration. Consider the second term on the right hand side.

Since

$$\int 2te^{\left(D_s\lambda_n{}^2+\frac{1}{\tau}\right)\cdot t} dt = 2\left[\frac{te^{\left(D_s\lambda_n{}^2+\frac{1}{\tau}\right)\cdot t}}{D_s\lambda_n{}^2+\frac{1}{\tau}} - \frac{e^{\left(D_s\lambda_n{}^2+\frac{1}{\tau}\right)\cdot t}}{\left(D_s\lambda_n{}^2+\frac{1}{\tau}\right)^2}\right], \quad (3.49)$$

and

$$\frac{1}{\tau}\int t^2 e^{\left(D_s\lambda_n{}^2+\frac{1}{\tau}\right)\cdot t} dt = \frac{1}{\tau}\left[\frac{t^2 e^{\left(D_s\lambda_n{}^2+\frac{1}{\tau}\right)\cdot t}}{D_s\lambda_n{}^2+\frac{1}{\tau}} - \frac{2}{\left(D_s\lambda_n{}^2+\frac{1}{\tau}\right)}\left(\frac{te^{\left(D_s\lambda_n{}^2+\frac{1}{\tau}\right)\cdot t}}{D_s\lambda_n{}^2+\frac{1}{\tau}} - \frac{e^{\left(D_s\lambda_n{}^2+\frac{1}{\tau}\right)\cdot t}}{\left(D_s\lambda_n{}^2+\frac{1}{\tau}\right)^2}\right)\right]. \quad (3.50)$$

Therefore,

$$C_n \cong \frac{2\cdot(-1)^n A e^{t/\tau}}{K\lambda_n}\left(\frac{t}{L^2\lambda_n{}^2+1}\right)$$

$$+ \frac{2\cdot(-1)^n B e^{t/\tau}}{K\lambda_n}\left(\frac{\tau}{L^2\lambda_n{}^2+1}\right)\left(2t+\frac{t^2}{\tau}-\frac{2t}{\left(L^2\lambda_n{}^2+1\right)^2}\right) + c_1 e^{-D_s\lambda_n{}^2 t}. \quad (3.51)$$

Using Eq. (3.42), we found $c_1 = 0$. Therefore,

$$C_n \cong \frac{2\cdot(-1)^n e^{t/\tau}}{K\lambda_n}\left(\frac{1}{L^2\lambda_n{}^2+1}\right)\cdot\left(At+2Bt\tau+Bt^2-\frac{2Bt\tau}{\left(L^2\lambda_n{}^2+1\right)^2}\right). \quad (3.52)$$

Consequently,

$$n(t,x) \cong At + Bt^2 + \sum_{n=1}^{\infty} \frac{2\cdot(-1)^n}{K\lambda_n}\left(\frac{1}{L^2{\lambda_n}^2+1}\right)\left(At + 2Bt\tau + Bt^2 + \frac{2Bt\tau}{\left(L^2{\lambda_n}^2+1\right)^2}\right)\cos(\lambda_n x)$$

$$= \left(At+Bt^2\right)\frac{\cosh(x/L)}{\cosh(K/L)} + 2Bt\tau\sum_{n=1}^{\infty}\frac{2\cdot(-1)^n}{K\lambda_n}\left(\frac{1}{L^2{\lambda_n}^2+1}\right)\left(1+\frac{1}{\left(L^2{\lambda_n}^2+1\right)^2}\right)\cos(\lambda_n x)$$

$$= \left(At+Bt^2\right)\frac{\cosh(x/L)}{\cosh(K/L)} + 2Bt\tau\left(\frac{\cosh(x/L)}{\cosh(K/L)}-1\right) + 2Bt\tau\sum_{n=1}^{\infty}\frac{2\cdot(-1)^n}{K\lambda_n}\frac{1}{\left(L^2{\lambda_n}^2+1\right)^3}\cos(\lambda_n x). \quad (3.53)$$

The second and third terms on the right hand side of Eq. (3.53) are very small compared to the first term. Therefore,

$$n(t,x) \cong \left(At+Bt^2\right)\frac{\cosh(x/L)}{\cosh(K/L)}$$
$$= k_a p_i l(111)_{VPD+Surf}\frac{\cosh(x/L)}{\cosh(K/L)}. \quad (3.54)$$

Compared with Eq. (3.31), Eq. (3.54) also predicts the thickness to be composed of two terms, i.e. the first term resulting from VPD effects and the other term resulting from SM effects. However, the surface contribution effects in Eq. (3.54) led the latter to depend on a square of growth time instead of being a linearly function as appearing in Eq. (3.31). This implies that the power function of time appearing in the latter term was governed by the function of *l*(111) growth rate. Also, it should be noted that Eqs. (3.54) and (3.29) suggest that *n*(*t*,*x*) can be written in the form of Eq. (3.30), i.e.

$$n(t,x) \cong k_a p_i \cdot l(111)\cdot\frac{\cosh(x/L)}{\cosh(K/L)}. \quad (3.55)$$

This suggests that the precursors' concentration on (001) surface depend linearly on the length of *l*(111).

However, the solution we have obtained so far results only when we neglect the decrease of the width of the opening stripes. As we are interested in the case of narrow stripes (width of the opening region is less than 10 μm), the decreasing of the opening width should be also taken into account. This lead the problem to be a partial differential equation subjected to time-dependent boundary condition:

$$\frac{\partial n}{\partial t} = D_s \frac{\partial^2 n}{\partial x^2} - \frac{n}{\tau}, \tag{3.56}$$

with

$$n\left(t, x = \pm\tilde{K}(t)\right) = k_a p_i \cdot l(111), \tag{3.57}$$

$$n(t = 0, x) = 0, \tag{3.58}$$

where $\tilde{K}(t) = K - l(111)cos\left(54.7^\circ\right)$ is a half of the actual opening region, i.e. a half of the opening region when the area of (111)B facets is also considered. Time dependent aspect appearing in Eq. (3.57) leads to a complicated problem which cannot be solved by using the same method. However, by using an approximation that the increasing of *l*(111) over time is small, the solution (3.55) can still be applicable. That is, the solution of Eqs. (3.56)-(3.58) can be approximate in the form of

$$n(t, x) \cong k_a p_i \cdot l(111) \cdot \frac{cosh(x/L)}{cosh\left(\tilde{K}(t)/L\right)}. \tag{3.59}$$

To analyze the error of Eq. (3.59), we substitute Eq. (3.59) into Eqs. (3.56)-(3.58). It can be seen that the solution satisfies the boundary conditions (3.57) and (3.58). However, an error occurs in Eq. (3.56) as

$$\begin{aligned}
\frac{d\Delta}{dt} &\propto \frac{dl(111)}{dt} - l(111) \cdot tanh\left(\tilde{K}/L\right) \cdot \frac{d\tilde{K}}{dt} \cdot \frac{1}{L} \\
&= \frac{dl(111)}{dt} \cdot \left[1 + \frac{l(111) \cdot tanh\left(\tilde{K}/L\right) \cdot cos\left(54.7^\circ\right)}{L}\right] \\
&= \frac{dl(111)}{dt} \cdot \left[1 + tanh\left(\tilde{K}/L\right) \cdot \frac{\left(K - \tilde{K}\right)}{L}\right] \\
&= \frac{dl(111)}{dt} \cdot \delta(t),
\end{aligned} \tag{3.60}$$

while the error of the solution (3.55) is

$$\begin{aligned}
\frac{d\Delta}{dt} &\propto \frac{dl(111)}{dt} \cdot \\
&= \frac{dl(111)}{dt} \cdot \delta(t),
\end{aligned} \tag{3.61}$$

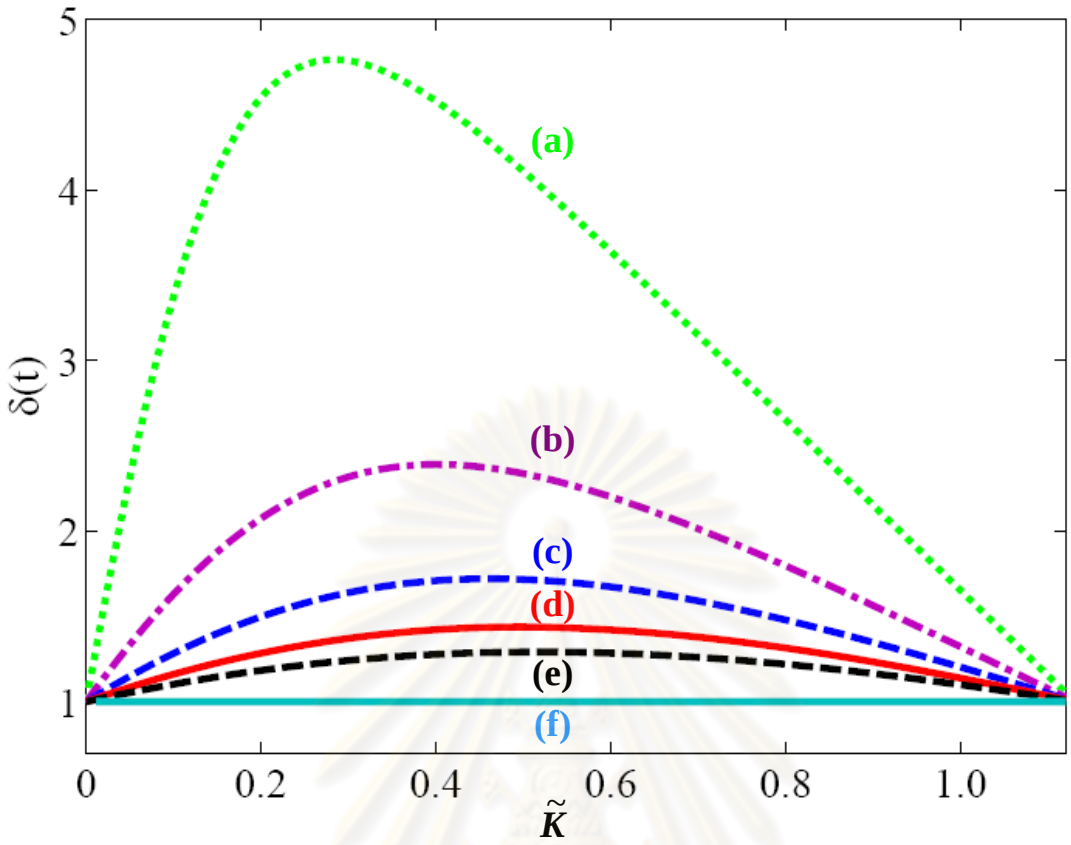


**Figs. 3.8 (a) - (e)** show the variation of function δ(t) appearing in Eq. (3.60) as a function of $\tilde{K}$ of the stripe with fill factor 0.35 ($K$ = 0.13 μm), which is the smallest fill factor of the samples used in our work. The function δ(t) in Figs. (a) to (e) were simulated at different values of $L$: 0.2, 0.4, 0.6, 0.8, 1.0 respectively. Figure (f) is the function δ(t) in Eq. (3.61), which is constant (equal to one), independent on $L$.

where δ(t) in Eq. (3.61) is constant (equal to one) and time independent for all $L$. The propagations of error in Eqs. (3.60) and (3.61) at different value of $L$ are shown in Fig. 3.8. Under this assumption that Eq. (3.59) is applicable, the thickness becomes

$$T(t,x) \cong r_g(x)t + \int_0^t \frac{k_g}{\tau} n_s(x,u)du$$

$$= r_g(x)t + \frac{k_g}{\tau} \cdot k_a p_i \cdot \int_0^t l(111) \cdot \frac{\cosh(x/L)}{\cosh(\tilde{K}/L)}du \qquad (3.62)$$

It can be seen that surface migration model contains two unknown parameters i.e. the surface migration length on (001) surface ( $L = \sqrt{D_s \tau}$ ) and the product of an adsorption constant ($k_a$), a partial pressure of group III precursors on (111)B facet ($p_i$), a molecular volume of the film ($k_g$), and an inverse of average lifetime of group III precursors on (001)

surface ($1/\tau$), i.e. $k_g k_a p_i/\tau$. For simplicity, the latter product will be named as the weight of surface migration contribution. Theoretically, surface migration length on (001) surface represents the distance that group III precursors can migrate from the edge to the inner region of (001) top surface. The weight of surface migration contribution indicates the extent of surface migration contribution on the film growth rate and thickness.

To further understand surface migration effects, surface migration model derived in this chapter will be applied to simulate the growth rate and thickness of c-GaN narrow stripes. The results and discussion will be shown in chapter 5. The thickness of the film will be calculated and compared with experimental results. The meaning of $L$ and the weight of surface migration contribution will be drawn, and the best-fit values for c-GaN narrow stripes in the considered growth condition will be given.

# CHAPTER IV

# VAPOR PHASE DIFFUSION MODEL: RESULTS AND DISCUSSION

The results simulated by using VPD model in conjunction with boundary conditions illustrated in the chapter 3 will be demonstrated and discussed. The goal of this chapter is to evaluate the capability of VPD model in SA growth with narrow stripe patterns and to understand the effects of VPD on growth rate and morphologies. Moreover, to understand the growth mechanisms in SA growth, physical meaning of the parameter in the model will be drawn and discussed.

## 4.1 Unknown parameters

To simulate growth rate profiles of SA c-GaN, VPD model was applied with a finite different method. During this stage, VPD will be taken as the only mechanism governing lateral movement of the Ga precursors from masks to the open windows under group-V-overpressure growth condition. Surface migration effect was ignored.

The concentration at a certain point in stagnant layer was calculated via a steady state differential equation in conjunction with proper boundary conditions as described in chapter 3.

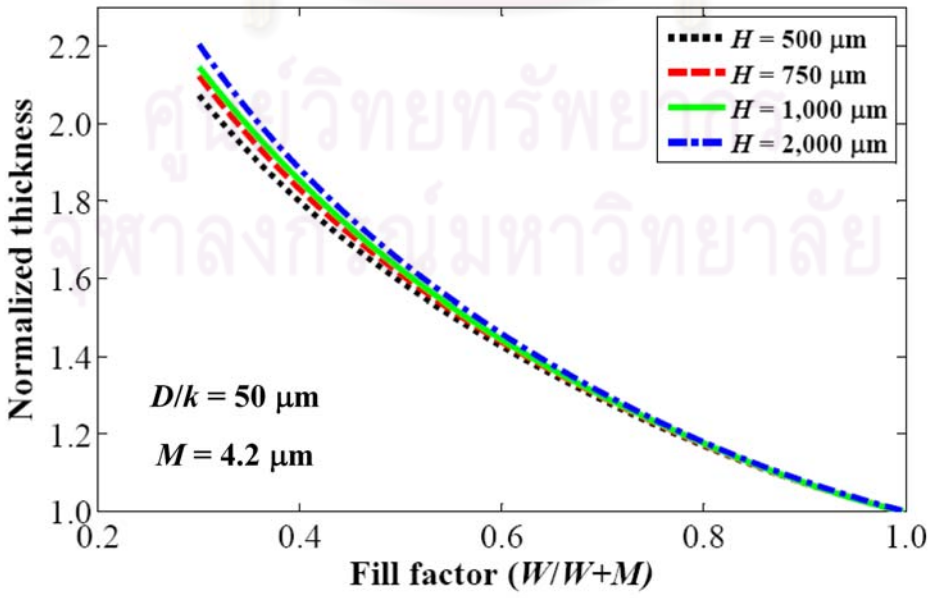


**Fig. 4.1** Normalized thickness profiles as a function of fill factor with typical values of *D/k* and mask width of 50 and 4.2 μm, respectively. *H* value was varied from 500 to 2,000 μm.

At top boundary of the stagnant layer, the concentration was fixed as a constant with independent of position and time. However, it is found that the height ($H$) of the stagnant layer must be high enough in order to suppress any distribution of the precursors at the boundary of the stagnant layer on the concentration's profile at the substrate surface.

We have used the height of the stagnant layer, $H$ = 1,000 μm, which is approximately 100 times wider than the period of stripe pattern with highest fill factor of 0.72. To justify its applicability, the value of $H$ was varied to analyze the upcoming results whether the variation of $H$ affects the concentration profile. Figure 4.1 shows normalized thickness via VPD model as a function of fill factor with typical value of $D/k$ and mask width of 50 μm and 4.2 μm, respectively. Value of $H$ was varied from 500 to 2,000 μm. It is seen that the variation of $H$ has a small influence on the thickness profile. An increase in $H$ results in an increase of thickness and tends to saturate at higher values (>1,000 μm). Thus, in order to further reduce the error, the value of $H$ in all calculations was fixed at 1,000 μm.

## 4.2 Steady state condition

In this section, we describe influence of iteration on concentration of Ga precursors, which is very alike to the case of growth proceed in a real growth process. Figure 4.2 shows concentration of Ga precursors at one position on the surface, increasing with iteration before getting saturated. During the first round, concentration of precursors just on the surface is very low. It is due to a limited number of precursors diffusing from the fluid layer and reaching the surface. As the iteration proceeds, more precursors can travel to the surface. This results in an increase of concentration on the surface. Saturation occurs when the rate of deposition equals the influx of precursors from the fluid layer. Thus, under saturation condition, concentration on the surface becomes saturate and iteration independent.

Concentration profile of the entire stagnant layer when the saturation occurs is shown in Fig. 4.3. The simulated concentration profile is of the stripes with fill factor 0.3, mask width 4.2 μm and $D/k$ of 50 μm.

Deposition rate at a certain position on the open surface, $r_g(x)$, can be drawn from the concentration profile through a linear proportional relation in the boundary condition: $r_g(x) = k u_{surf}(x)$. Note that the deposition rate on masks was set to be zero by the boundary

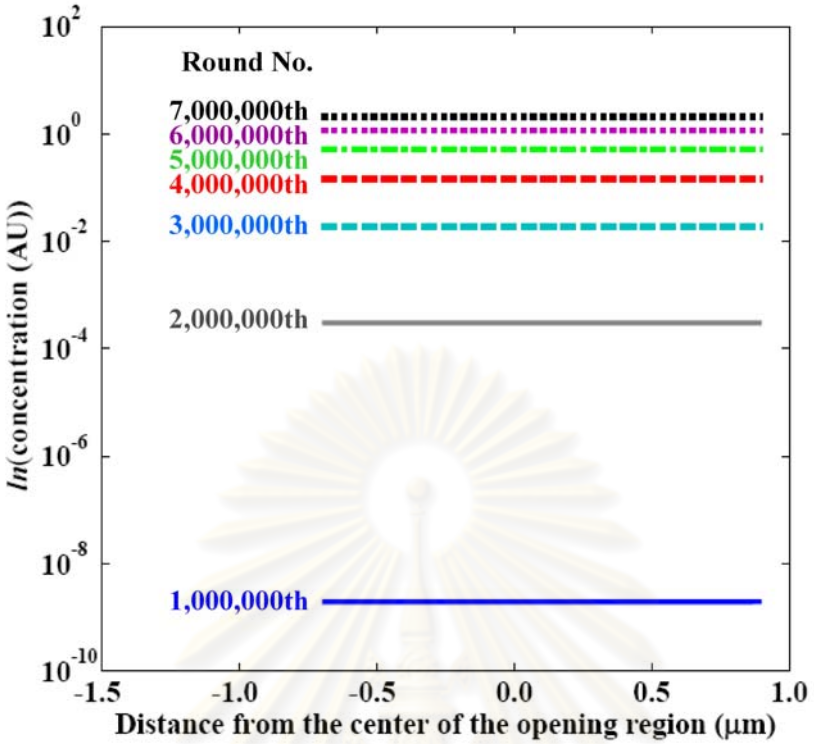


**Fig. 4.2** Typical logarithm of the concentration on the surface as iteration proceeds. Fill factor, mask width and *D*/*k* used in this simulation are 0.3, 4.2 and 50 μm, respectively.

condition of the model. To calculate the film thickness at a certain growth time, we make a simplification by assuming time independent growth rate. Under these assumptions, thickness as a function of fill factor can be obtained from

$$T(t,x;FF) = t \cdot r_g(x;FF) = t \cdot ku_{surf}(x;FF)\ , \qquad (4.1)$$

where *FF* is fill factor.

Concerning the problem of using arbitrary units from simulated values and the problem of how to fit the simulated results with experimental results, we normalized the simulated concentration for each fill factor by the simulated concentration at fill factor 1.00 or no-mask condition. Thus, the final concentration, which is plotted in the figure, has no unit. Substituting this unitless concentration into Eq. (4.1), we obtain a unitless thickness, namely normalized thickness.

$$T_{norm}(t,x;FF) = \frac{t \cdot ku_{surf}(x;FF)}{t \cdot ku_{surf}(x;FF=1)} = \frac{u_{surf}(x;FF)}{u_{surf}(x;FF=1)}\ . \qquad (4.2)$$

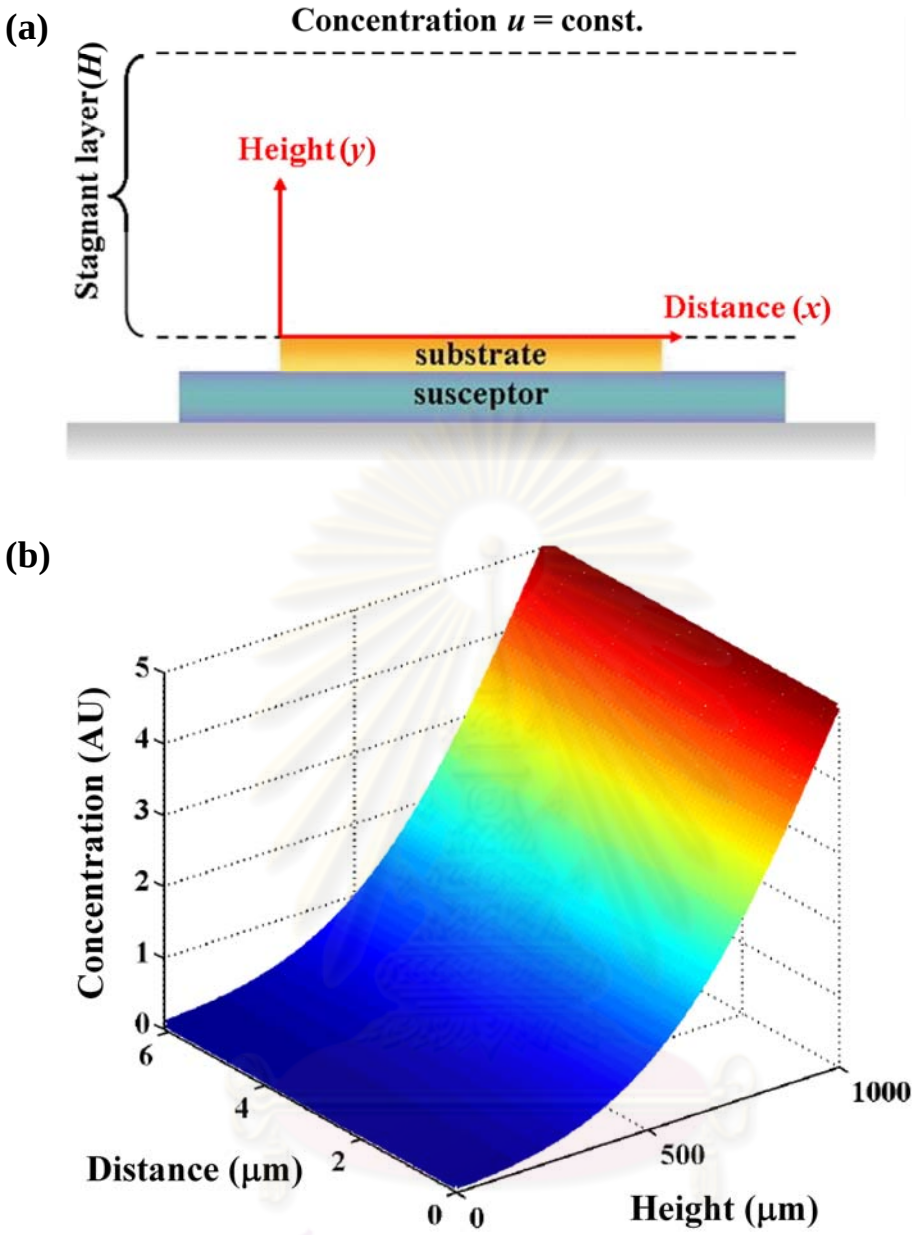


**Fig. 4.3 (a)** Schematic diagram of the stagnant layer and **(b)** the concentration profile in the stagnant layer when saturation occurs

## 4.3 Fill factor dependent thickness

Fill factor - defined as a ratio of the opening width to the pattern period - was observed to have profoundly effects on the growth rate of selective area c-GaN narrow stripes. As shown in chapter 3, a decrease in fill factor significantly raised the growth rate of the stripes. This is because the decrease in fill factor is the increase of the area covered with dielectric masks and therefore leads to higher accumulation of the precursors above the masks, on which

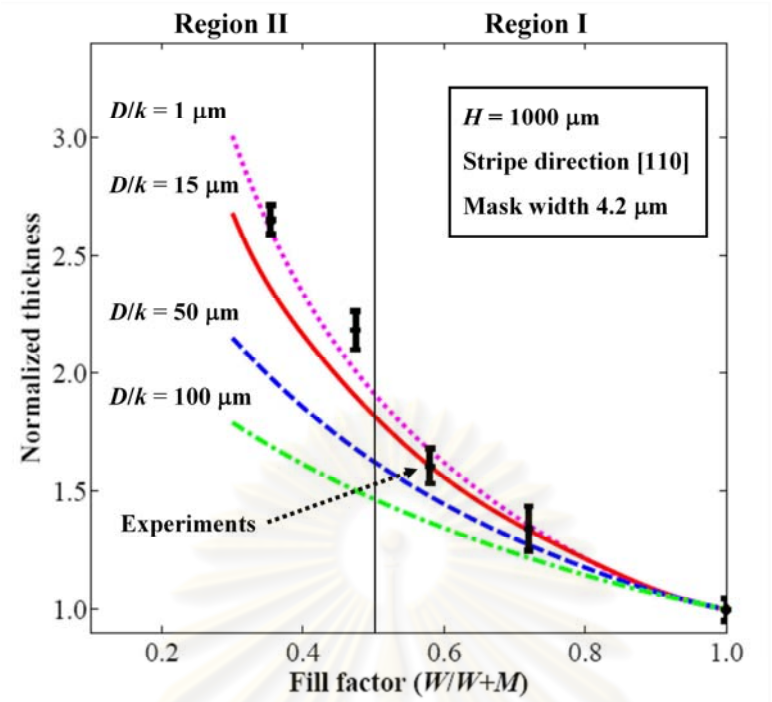


**Fig. 4.4** Normalized thickness profiles of measured (stars) and simulated (lines) results of c-GaN stripes along the [110] direction as a function of fill factor.

no deposition can occur. Higher concentration gradients occur between masks and opening regions in between, on which the concentration of the precursors depletes due to the deposition of the gaseous precursors into solid compound. These higher concentration gradients lead to stronger lateral flux of precursors from above the masks to the opening regions and subsequently result in an enhancement of the growth rate on the opening regions.

To quantitatively analyze the effect of fill factor on growth rate enhancement, VPD model was applied to simulate the normalized thickness profile at different growth condition, i.e. at different $D/k$. The simulated results are shown compared to experimental data in Fig. 4.4. The measured values were labeled by black stars with error bars, and the simulated normalized thickness profiles from VPD model were labeled by lines. Those normalized thicknesses were calculated by using Eq. (4.2), where the initial thickness was calculated from the concentration on the surface at the center of the opening region. As the normalized thickness has the same meaning as a multiple of growth rate enhancement, from now on we will call it shortly as growth rate enhancement (GRE).

In Fig. 4.4, it can be seen that GRE of small fill factor increases strongly with the decreasing of fill factor. When comparing the experimental results to the simulated ones, we

observed that the correlation between the GRE and the fill factor divided itself into two regions: the region of fill factors higher and smaller than 0.5 (0.5 is a roughly approximated value). In region I (fill factor greater than 0.5), the GRE of selective area c-GaN is found to agree very well with the simulated results from VPD model for $D/k$ = 15 μm. In region II (fill factor smaller than 0.5), on the other hand, the experimental GREs are considerably higher than those predicted by VPD model with $D/k$ = 15 μm. The deviation suggests a reduction of a proper $D/k$ to be only a few micrometers. However, we have tried to improve the correlation by decreasing $D/k$ below 1 μm but nevertheless we found that the profile of normalized thickness cannot be raised higher than the profile simulated with $D/k$ = 1 μm, since the profile saturated. This deviation, therefore, indicates the limit of an application of VPD model for selective area growth of narrow stripes.

Concerning a possible source of this deviation, we believed that the neglect of surface migration process had caused this effect. That is, the trend of GRE in the region I (fill factor smaller than 0.5) cannot be explained by considering only the effects of vapor phase diffusion process. The deviation suggests non-negligible effects of surface migration process. Therefore, the difference between the simulated results with $D/k$ = 15 μm and the experimental data indicates the extent of the contribution of the surface migration process. These results also suggest that fill factor can be used as a tool to distinguish the starting point at which surface migration process significantly takes effect.

## 4.4 *D/k* dependent growth profiles

We have found that $D/k$ has influences both on the surface profile i.e. curvature of the film surface and on the growth rate enhancement of the film. To understand the physical meaning of $D/k$ on the film surface, cross-sectional normalized thickness profiles of c-GaN stripes with fill factor 0.58 at different $D/k$ are shown in Fig. 4.5. It can be observed that the simulated film with $D/k$ higher than 50 μm has a rather planar surface, while curved surface profiles was obtained for $D/k$ smaller than 50 μm. Moreover, as increasing fill factor, the film surface tends to be more curved as shown in Fig. 4.6 (a), which demonstrates the comparison between the simulated normalized thicknesses at the center and edges of the opening region as a function of fill factors. The percent of difference between those two regions was also calculated and shown in Fig. 4.6 (b). It should be noted that the normalized thickness used in

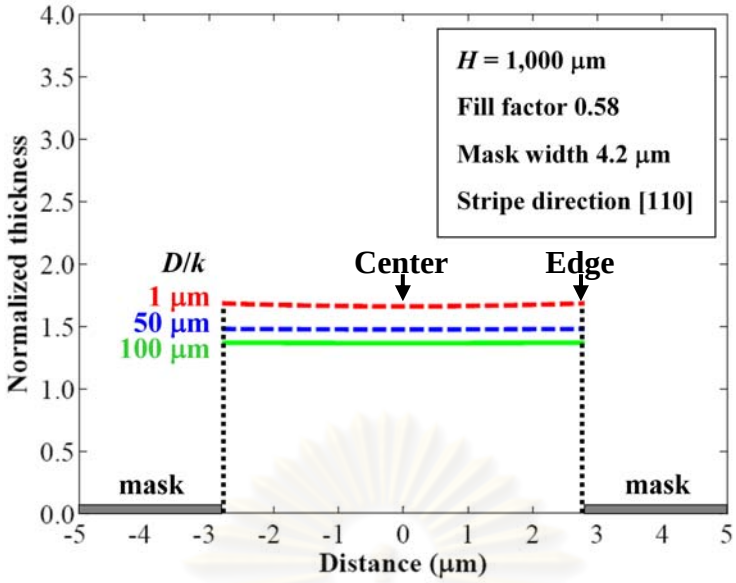


**Fig. 4.5** Simulated cross sectional picture of c-GaN stripes at *D*/*k*: 1, 50, 100 μm.

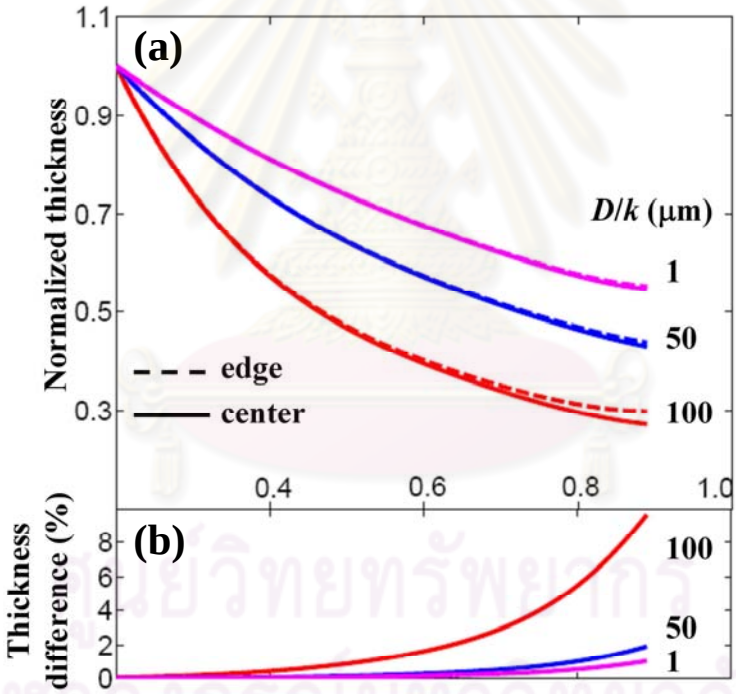


**Fig. 4.6 (a)** The difference in normalized thickness at the center and edge of the opening region and **(b)** A percent of difference in the thickness at center and edge of the opening region as a function of fill factors at *D*/*k*: 1, 50 and 100 μm

Figs 4.6 (a) and (b) was defined differently from the normalized thickness defined in Eq. (4.2). For ease of demonstration, the normalized thickness at a certain fill factor in these two figures is defined as a ratio of the thickness at that fill factor to the thickness at fill factor 0.2, the smallest fill factor used in this case.

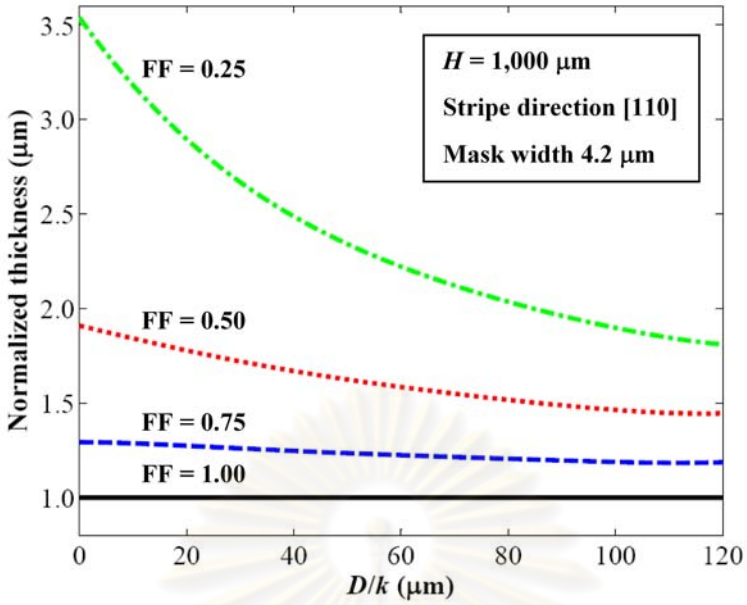


**Fig. 4.7** Simulated normalized thickness at the center of window region as a function of *D*/*k* at fill factors (FF): 0.25, 0.50, 0.75 and 1.00.

Figs. 4.5, 4.6 (a) and (b) indicate that the difference in GRE between the edges and the center lessens as the *D*/*k* increases. This implies that the precursors can diffuse with longer distance when *D*/*k* increases. The parameter *D*/*k*, which has a unit of length, can therefore be interpreted as an effective diffusion length of the Ga precursors. Note that, however, the effect of *D*/*k* on the surface profile is too small to take account of the actual surface profile observed in experimental c-GaN stripes in which the appearing of edges is very distinctive.

To examine the effects of *D*/*k* on the growth rate enhancement of selective area growth, the normalized thickness profile at constant fill factor as a function of *D*/*k* was observed. The results are shown in Fig. 4.5. In this simulation, the values of *D*/*k* were varied from 100 μm to approach zero. The fill factors were fixed at 0.25, 0.50, 0.75 and 1.00, and the mask width was fixed at 4.2 μm.

As shown in Fig. 4.5, at constant fill factor, the increase in *D*/*k* leads to a decrease of normalized thickness or GRE. This phenomena results from the fact that increasing *D*/*k* reduces the influence of the presence of masks on the opening regions, as the increasing of *D*/*k* gives the precursors higher mobility to diffuse from mask to opening regions. The increasing of *D*/*k* then lessens the accumulation of the precursors on masks and subsequently

reduces GRE. However, as can be observed from Fig. 4.7, the increasing of $D/k$ was found to have smaller effects on selective area growth with higher fill factor.

To link the actual growth condition to the parameter $D/k$, we need to know how $D$ and $k$ relate to the growth parameters such as total pressure, temperature, type of precursors. According to kinetic theory, $D$ relates to the growth parameters via

$$D_s = \frac{3}{8}\left(\frac{\pi k_B T}{2}\frac{m_1 + m_2}{m_1 m_2}\right)^{1/2}\frac{k_B T}{\sigma P} \tag{4.3}$$

where $k_B$ is Boltzmann's constant, $T$ is the temperature of the surroundings, $m_1$ and $m_2$ are the masses of the two type of precursors, $\sigma$ is the collision cross section and $P$ is the total pressure [44]. The relation between $k$ and the actual growth parameters is however much more complex. The constant involves many various chemical reactions, which is still under study. In our case, the effect of $D/k$ on actual growth conditions can not be study much further than this, as we lack experimental data of the growth at different growth conditions.

## 4.5 Summary

Vapor phase diffusion model was applied to the case of selective area growth of narrow stripes (mask width was fixed at 4.2 μm) to analyze the effects of vapor phase diffusion process. Even though the model is based on steady state equations, time dependent aspect still appeared through the results at different rounds of iteration. Despite of being applied on a narrow stripe case, the model was found to agree very well for the film with fill factor higher than 0.5 where the best-fit $D/k$ was found to be 15 μm. For smaller fill factor, surface migration process was found to have non-negligible effects and therefore must be concerned. For better understanding, the effects of the only parameter in the model, $D/k$, were studied. The parameter was found to indicate the precursor mobility and consequently interpreted as an effective diffusion length of group III precursors. However, the effect of $D/k$ was found to be too small to explain the morphology on the film surface. Surface migration is therefore required for the study of the surface morphology for narrow stripe selective area growth.

# CHAPTER V

# SURFACE MIGRATION EFFECTS: RESULTS AND DISCUSSION

In this chapter, the results simulated using VPD model with an addition of SM effects are discussed. The influence of surface migration process on the thickness of SA GaN narrow stripes along [110] direction was analyzed by varying the parameters in SM model, namely the surface migration length ($L$) and the weight of surface migration contribution, which is defined as the product of an adsorption constant ($k_a$), a partial pressure of group III precursors on (111)B facet ($p_i$), a molecular volume of the film ($k_g$) and an inverse of average lifetime of group III precursors on (001) surface ($1/\tau$), i.e. $k_g k_a p_i/\tau$. Physical meaning of these parameters is drawn and interpreted.

## 5.1 Calculation procedures in surface migration model

Surface migration model is a model which concerns both time dependent and time independent aspects of SA-MOVPE process. To obtain the film thickness and growth rate, VPD model must be applied first and then its results are then used in the SM model. The film thickness for each fill factor was calculated via,

$$\begin{aligned} T(t,x) &\cong r_g(x)t + \int_0^t \frac{k_g}{\tau} n_s(x,u)du \\ &= r_g(x)t + \frac{k_g}{\tau} \cdot k_a p_i \cdot \int_0^t l(111) \cdot \frac{\cosh(x/L)}{\cosh(\tilde{K}/L)} du \ , \end{aligned} \tag{3.62}$$

where $l(111)$ is an inclined length of (111) facets and $\tilde{K}$ is a half of (001) top surface length as shown in Fig. 3.7. For simplicity, from now on the product $k_g k_a p_i/\tau$, which was named as the weight of surface migration contribution, will be symbolized shortly by *weight*. Consequently, Eq. (3.62) can be rewritten as

$$\begin{aligned} T(t,x) &\cong r_g(x)t + \int_0^t \frac{k_g}{\tau} n_s(x,u)du \\ &= r_g(x)t + weight \cdot \int_0^t l(111) \cdot \frac{\cosh(x/L)}{\cosh(\tilde{K}/L)} du \ , \end{aligned} \tag{5.1}$$

where it should be noted that the parameters $l(111)$ and $\tilde{K}$ depend linearly on the thickness as

following,

$$l(111) = T(t, x = 0) / \sin(54.7^\circ), \tag{5.2}$$

and

$$\begin{aligned} \tilde{K}(t) &= K - l(111)\cos(54.7^\circ) \\ &= K - T(t, x = 0)\cot(54.7^\circ). \end{aligned} \tag{5.3}$$

Therefore, to obtain the thickness in Eq. (5.1), the thickness at the center of an open window i.e. at $x$ = 0 must be known before hand. To obtain the thickness at the center, we differentiated Eq. (5.1) once and obtained

$$\frac{\partial T(t)}{\partial t} = r_g\big|_{x=0} + weight \cdot l(111) \cdot \frac{1}{\cosh(\tilde{K}/L)}, \tag{5.4}$$

where $T(t)$ is thickness at the center of an open window ($x$ = 0) at time $t$. Then, by using Fourth-order Runge-Kutta Method, the thicknesses at the center of an open window as a function of time and fill factor were obtained. During each round of numerical calculations, the value of $\tilde{K}$ was computed, as the thickness must be calculated only from a non-zero $\tilde{K}$. This is because, when $\tilde{K}$ becomes less than or equal to zero, lateral overgrowth, i.e. the second growth process in the two-step growth model described in chapter 3, must be concerned. To calculate surface profile of SA c-GaN stripes, the thickness obtained from Eq. (5.4), namely the thickness at $x$ = 0 as a function of time and fill factor, was substituted into Eq. (5.1). Equation (5.1) was then solved via Newton-Cotes integration formula with $N$ = 6 [45].

## 5.2 Addition of surface migration effects

The thickness profile as a function of fill factor at growth time of 15 minutes calculated from VPD model with $D/k$ = 15 μm was shown in Fig. 5.1 (solid line). Those simulated thicknesses were the thickness at the center of an open window. The thickness profile was observed to divide itself into two regions as appearing in chapter 3. The simulated result fits very well to the experimental data (green circles with error bars) for fill factor higher than 0.5 (rough approximated value), but deviated from the experiments in the region of smaller fill factors. As discussed in chapter 3, we believed that the deviation results from

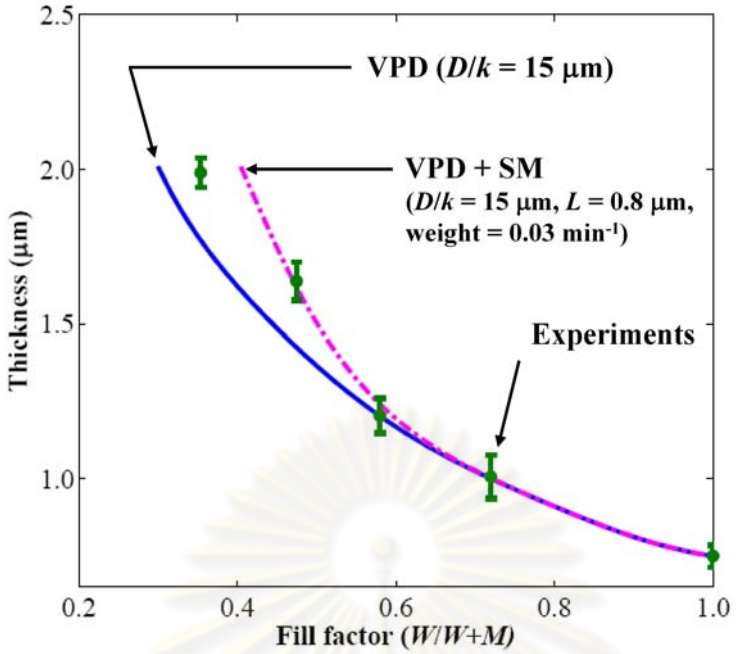


**Fig. 5.1** Simulated thickness profiles at the center of window region for growth time of 15 minutes from VPD model ($D/k$ = 15 μm) and VPD model ($D/k$ = 15 μm) including SM model ($L$ = 0.8 μm, *weight* = 0.03 $min^{-1}$) in compared with experimental data.

lack of surface migration effects. To prove that lack of surface migration effects is the factor that takes responsible for the deviation, the result from VPD model with $D/k$ = 15 μm was applied into Eq. (5.4), and the film thicknesses resulting from VPD and SM effects from the appearing of (111)B facets for all fill factors were calculated.

As can be observed in Eqs. (5.1) and (5.4), there are two unknown parameters getting involved in the calculation, namely the surface migration length on (001) surface ($L$) and the weight of surface migration contribution (*weight*). By varying these two parameters, we found that the thickness profile agreed well with the experimental data when $L$ = 0.8 μm and $weight = 0.03\,min^{-1}$ were used as shown in Fig. 5.1 (dash-dot line).

Note that surface migration contribution significantly raises the thickness profile calculated from VPD model and improves the agreement between the simulated and experimental results. The effects of surface migration in the region of small fill factors are therefore non-negligible as we had expected. Moreover, it should be noted that at the growth condition in use the contribution of surface migration effects starts to be noticeable at fill factor higher than we had roughly approximated. That is, the effects of contribution start to be

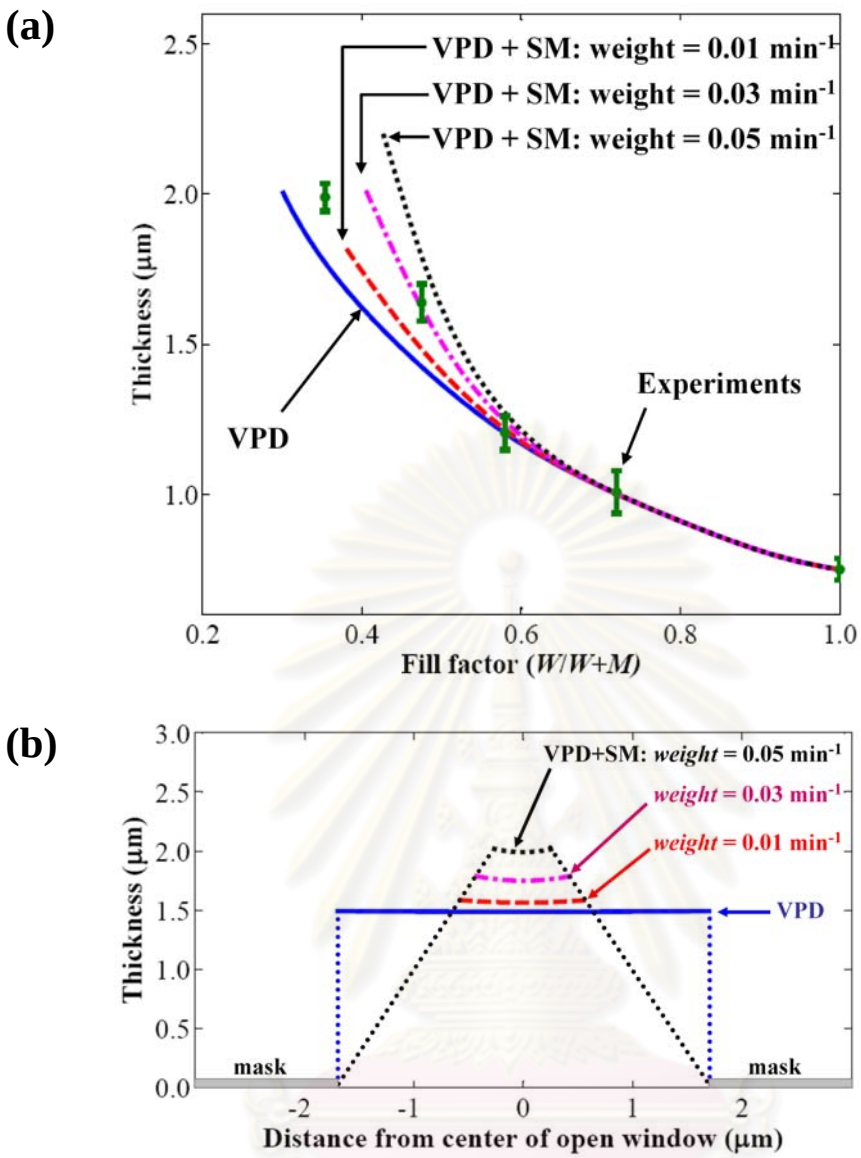


**Fig. 5.2 (a)** Simulated thickness profiles at the center of window region as a function of fill factor and **(b)** cross section of the film at fill factor 0.45 derived from VPD model and VPD model including SM model in compared with experimental data. In these figures, *D*/*k* and *L* were fixed at 15 and 0.8 μm, respectively. The *weight*, on the other hand, was varied at 0.01, 0.03 and 0.05 $min^{-1}$.

noticeable at fill factor ~ 0.63. Moreover, the results also suggested that, at the growth time being used (15 min), (111)B sidewall facets starts to merge at fill factor ~ 0.40.

## 5.2.1 Effects of weight of contribution on thickness and surface profiles

To further analyze the effects of surface migration process, we varied the value of *weight* while fixed the value of *L* at 0.8 μm (the best-fit value). The simulated thicknesses at the center of an open window for all fill factors were taken. The consequent thickness profiles

over fill factor are shown in Fig. 5.2 (a). The increase of *weight* was observed to have an effect in raising the thickness profile at fill factors smaller than 0.63, while for higher fill factors the thicknesses remain at the same value. The increasing of thickness also leads the sidewall merging to occur up into higher fill factors.

To understand the effects of the weight on the film surface profiles, we considered the simulated cross section as *L* was fixed and the weight was varied. The results are shown in Fig. 5.2 (b). In this figure, the fill factor of the film is 0.45, the mask width is 4.2 μm and *L* was fixed at 0.8 μm (the best-fit value). As shown in Fig. 5.2 (b), the increase of *weight* leads to an increasing of thickness everywhere above the open window. The increasing of thickness at all position above the opening window is therefore a probable cause that leads the merging of (111)B sidewalls to occur at higher fill factor. Also, the increasing of weight leads to the occurrence of growth rate enhancement at edges.

These results suggest that the weight governs the extent of contribution but do not have any influence on the ability of the precursors to move along the surface. The latter conclusion came from the results shown in Fig. 5.2 (b). As the weight increases but *L* is fixed, the surface profile will become more curves. This suggests that more precursors migrating to the top surface but can not move far enough. Therefore, they accumulate near the edges.

## 5.2.2 Effects of surface migration length

To study the effect of *L*, the weight of contribution was fixed at 0.03 $min^{-1}$ (the best-fit value), while *L* was varied. The simulated thicknesses at the center of an open window were taken, and the results are shown in Fig. 5.3 (a). As shown in Fig. 5.3 (a), the increase of *L* also leads to an increase in thickness. Therefore, the occurrence of (111)B sidewalls merging was observed at higher fill factor. Interestingly, the point where the surface migration contribution starts to be noticeable is also affected by varying *L*.

Figure 5.3 (b) shows the simulated film cross section when the weight was fixed at 0.03 $min^{-1}$ (the best-fit value) and *L* was varied. In this figure, the fill factor is 0.45, mask width is 4.2 μm as in Figure 5.3 (a) and weight is at 0.03 $min^{-1}$. It can be seen that the increasing of *L* causes higher thickness everywhere on the open window. Moreover, the surface becomes more planar with increasing of *L*.

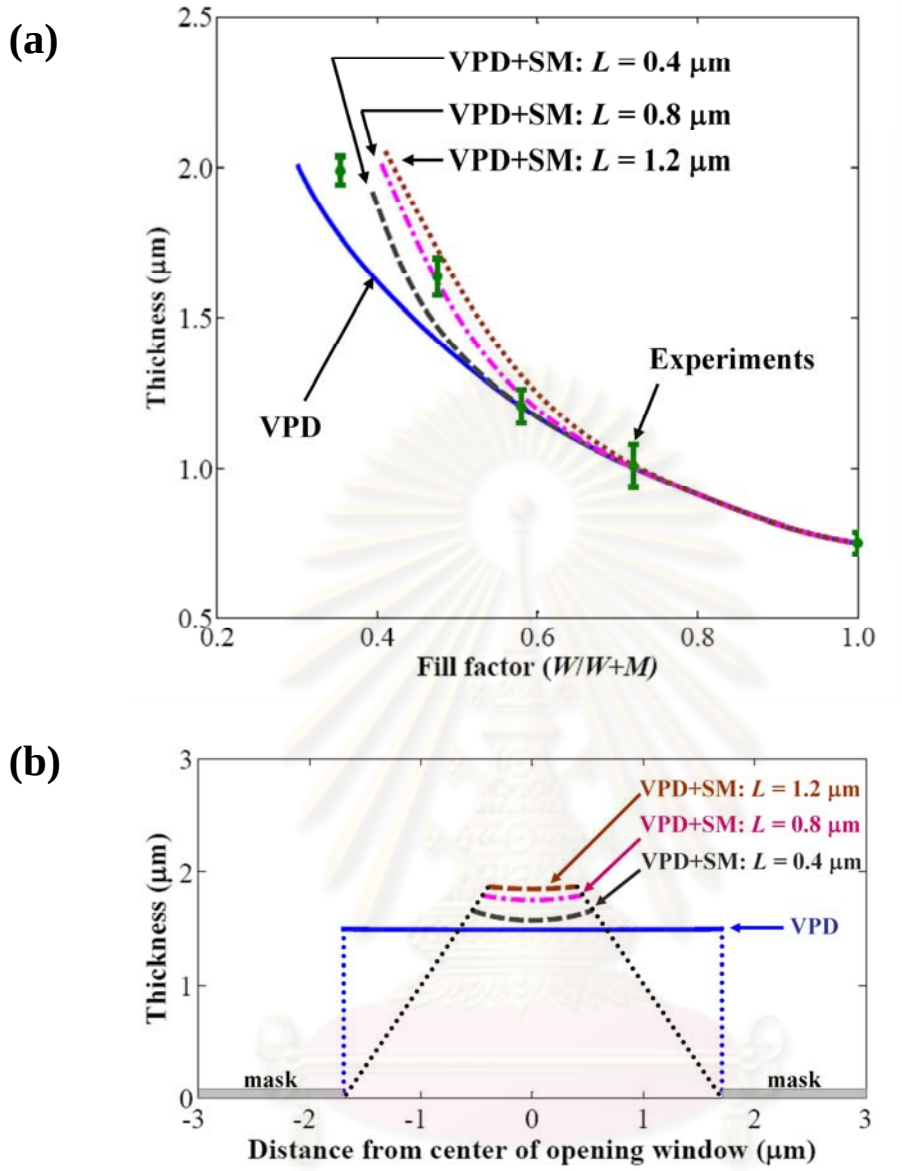


**Fig. 5.3 (a)** Simulated thickness profile at the center of window region and **(b)** cross section at fill factor 0.45 from VPD model ($D/k$ = 15 μm) and VPD model ($D/k$ = 15 μm) including SM model in compared with experimental data. In these figures, the *weight* was fixed at $0.03\,min^{-1}$, while $L$ was varied at 0.4, 0.8 and 1.2 μm.

The results suggest that $L$ influences strongly on precursors' mobility in the way that increasing $L$ gives the precursors higher mobility. This higher mobility therefore results in an increasing of thickness everywhere on the surface because more precursors can move from (111)B sidewalls onto the top surface. Moreover, this higher mobility also flattens the top surface as the precursors have enough mobility to move away from the edges.

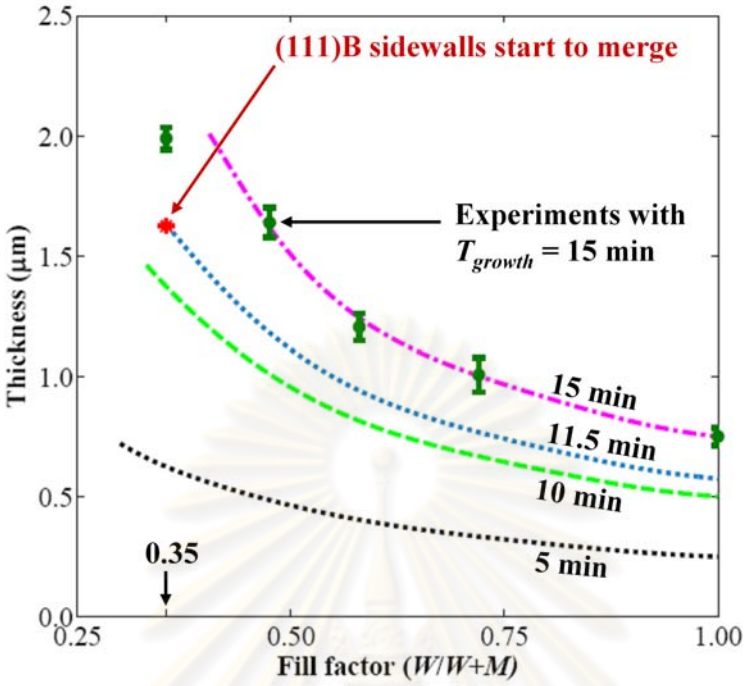


**Fig. 5.4** Simulated thickness profiles at the center of window region with various growth time of 5, 10, 11.5 and 15 minutes from VPD model ($D/k$ = 15 μm) including SM model with $L$ and *weight* of 0.8 μm and 0.03 $min^{-1}$ in compared with experiments

## 5.3 Growth time and thickness profiles

To study the effect of growth time on the thickness profiles, we simulated the film at all fill factors at different growth times: 5, 10 and 15 minutes. The thickness at the center of an open window was taken and the profiles of thickness at different growth time are shown in Fig. 5.4. The film at higher fill factor (fill factor closer to 1.00) was observed to have lower time dependence on the growth rate and it can be seen that at fill factor 1.00, the film has completely constant growth rate. At lower fill factor, the merging of (111)B was observed. At growth time of 5, 10 and 15 minutes, it can be seen that the (111)B sidewalls merging occurs for all of the film with fill factor lower than 0.30, 0.33 and 0.40, respectively. The thicknesses at the fill factor lower than such values are therefore influenced by lateral overgrowth process, the second growth process in our two-step growth model. In our c-GaN film with lowest fill factor (0.35), we also found that the merging starts to occur at growth time of 11.5 minutes.

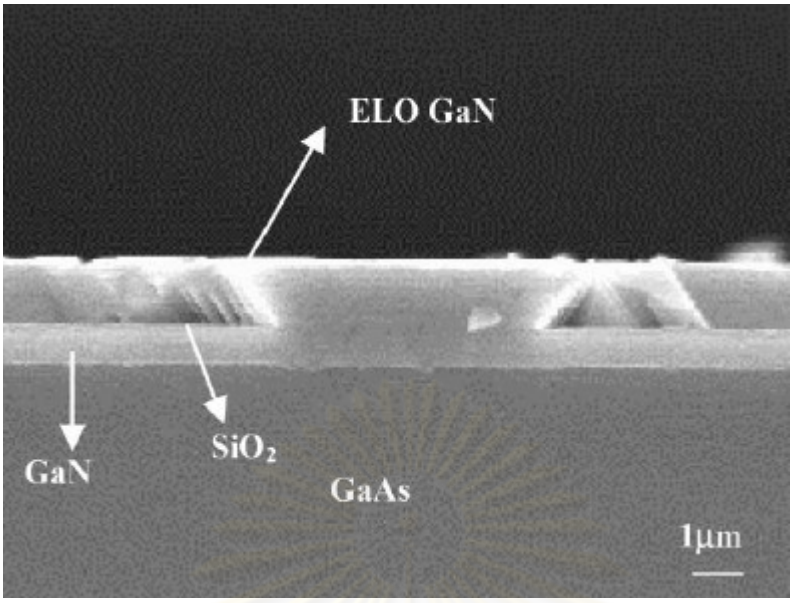


**Fig. 5.5** Cross sectional image of c-GaN stripe oriented along the [1-10] direction. [46]

## 5.4 Effects of surface migration on the film with cross sectional shape of upside down trapezoid

From literature review, we found that c-GaN stripes with (111)B sidewalls at a different growth condition can also have another type of cross sectional shape. Figure 5.5 shows a picture of c-GaN stripe cross section taken from an article of Fu *et al*. [46]. The strips oriented along [1-10] direction, which is 90 degrees different from our growth conditions. As can be observed in Fig. 5.5, the film has a rather planar (001) top surface. To examine if surface migration process can explain such a profile and also to find out the growth parameters of such surface, we tried the simulation with various values of *L* and *weight*. The results are shown in Figs. 5.6 (a) and (b).

Figures 5.6 (a) and (b) show the simulated film cross sectional shape when the *weight* and *L* were fixed at 0.015 $min^{-1}$ and 0.8 μm in compared with the shape calculated by using only VPD model. In this figure, the fill factor was 0.45, the mask width was 4.2 μm and *D*/k was 15 μm. The simulated film with a rather planar top surface is obtained with small value of *weight* in conjunction with high value of *L*. This suggests that surface migration process has very small effects on such a shape. However, since there are many different growth parameters between our case and Fu *et al*.'s case, we can not conclude what the most probable

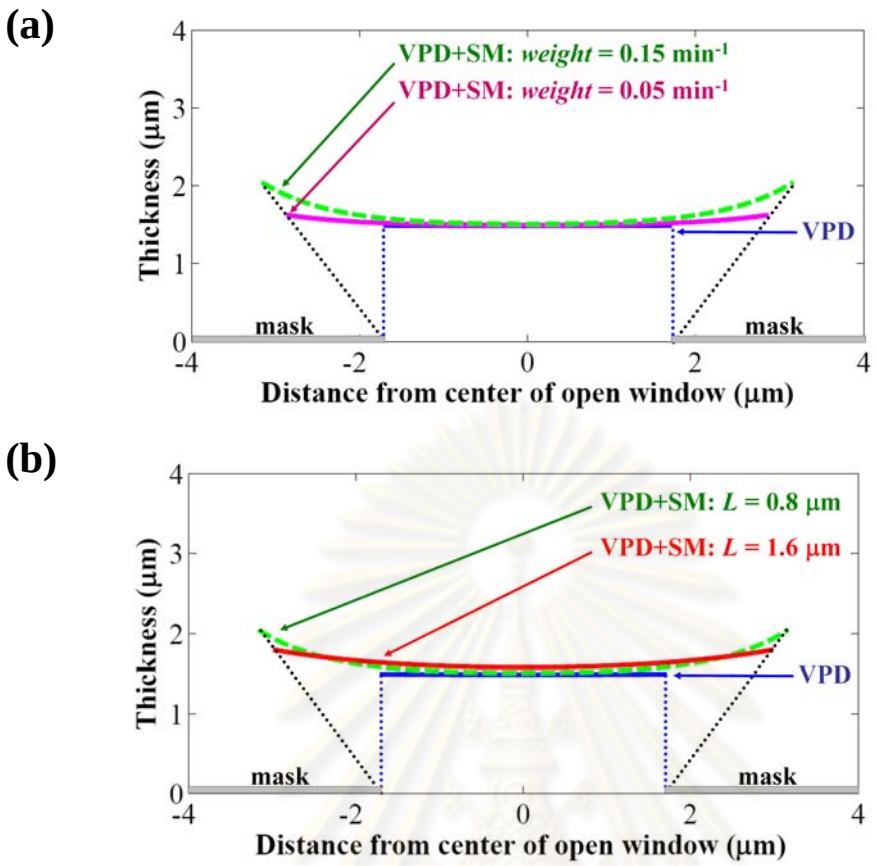


**Fig. 5.6 (a)** and **(b)** cross section from VPD model ($D/k$ = 15 μm) and VPD model ($D/k$ = 15 μm) including SM model. In figure (a), $L$ was fixed at 0.8 μm, while *weight* was varied at 0.005 and 0.015 $min^{-1}$. In figure (b), *weight* was fixed at 0.015 $min^{-1}$, while $L$ was varied at 0.8 and 1.6 μm.

cause of this phenomenon is. In order to understand further, we need to know the relation between $L$ and other growth parameters. However, the dependence of the surface migration length $L$ which was defined as $L = \sqrt{D_s \tau}$ and actual growth parameters such as growth temperature, total pressure, type of the sources of precursors is still unknown. Lebedev *et al.* reported that the diffusion length on Ga-face GaN that an atom travels within the coalescence time can be obtained via [47]

$$L = \sqrt{\frac{k_B T}{C\gamma}} \left( \frac{R}{a} \right)^2, \tag{5.5}$$

where $k_B$ is Boltzmann's constant, $T$ is the temperature, $R$ is the domain radius ~ 250 nm, γ is the surface energy, $C$ is a numerical constant ~ 25, and $a$ is the atomic dimension ~ 0.3 nm. However, the information about cubic phase GaN is still lacked. The relation between those

parameters in Eq. (5.5) and temperature is therefore still unknown for our case and more study about the growth of cubic GaN is needed.

## 5.5 Summary

In this chapter, we applied surface migration model to the results of vapor phase diffusion model in chapter 4. The addition of surface migration effects with *weight* and *L* of 0.03 $min^{-1}$ and 0.8 μm was found to improve the correlation between experimental data and simulation. Surface migration was shown to be non-negligible for the film with small fill factor. The parameters of the model: surface migration length, *L*, and weight of contribution, *weight*, were also interpreted. Surface migration length was found to govern the precursors' mobility to move on the top surface in such a way that an increase of surface migration length leads to higher mobility. The weight of contribution has influences on the extent of surface migration contribution. The increasing of weight results in higher contribution of surface migration effects. Surface migration effects are also dependent on time. The occurrence of (111)B sidewalls merging in our c-GaN film with smallest fill factor (0.35) was found to occur prior to 15 minutes. To calculate the thickness of the film, lateral overgrowth process must be concerned. The film with upside down trapezoidal cross sectional shape was also considered. The profiles suggest that in such a case surface migration length was high, while the weight of contribution was small. These condition leads to a rather planar top surface as appearing in the actual film.

# CHAPTER VI
# CONCLUSION

Growth mechanism of selective area metalorganic vapor phase epitaxy (SA-MOVPE) and its effect on the thickness and morphologies of SA c-GaN narrow stripes were analyzed by using diffusion models, namely vapor phase diffusion (VPD) and surface migration (SM) models. The physical meaning of parameters used in these models was drawn and interpreted. Subsequently, a way to reduce the hexagonal inclusion in c-GaN, which was usually observed in SA c-GaN films, was also suggested. A brief results and discussion of the study are as follows.

Firstly, VPD model was applied to the case of selective area growth with narrow stripes (mask width of 4.2 μm). The simulated results were found to agree very well for the film with fill factor higher than 0.5, and the only parameter in the model, namely $D/k$ which is the ratio of the diffusion coefficient to the deposition rate constant, was found to be best fitted at the value of 15 μm. For smaller fill factor, the deviation between the experimental data and the simulation results was found. Therefore, surface migration effects were found to be non-negligible in that range of fill factors. The parameter $D/k$ was observed to affect the precursors' mobility. The parameter was interpreted as the effective diffusion length of group III precursors in gas phase. However, the effects of $D/k$ were found to be too small to explain the morphology of the film surface as observed in the experiments. Surface migration was believed to be cause of the inconsistencies found in the study.

With the addition of surface migration effects, an improvement of the correlation between experimental data and simulation was observed. The lack of surface migration effects was therefore proved to be the cause of the deviation between the simulation results from VPD model and the experiments in the range of small fill factors, and surface migration process was therefore non-negligible in the case of fill factor smaller than 0.5. The best-fit value of the SM model's parameters, namely the weight of contribution (*weight*) and the surface migration length ($L$), were found to be 0.03 $min^{-1}$ and 0.8 μm respectively. Also, the surface migration effects were observed to be high enough to govern the feature observed in the experimental surface morphologies of c-GaN. The physical meaning of the parameters in

the model was also interpreted. *L* was found to have effects on the precursors' mobility to move on the top surface in such a way that an increase of *L* gave the precursors' higher mobility to move on the surface. Therefore, the surface profile with higher value of *L* was observed to be more planar and the thickness was observed to increase with the increase in *L*. The *weight*, on the other hand, had influences on the extent of surface migration contribution such that the increasing of *weight* resulted in higher contribution of surface migration effects, and therefore led to higher thickness everywhere on the top surface. Also, surface migration effects were observed to be time dependent.

Besides its dependence on fill factor, *weight* and *L*, the growth rate of the film was found to be varied with time. Our calculation suggested that the occurrence of (111)B sidewalls merging of our c-GaN film with fill factor 0.35 occur prior to 15 minutes. To calculate the thickness of the film in this case, lateral overgrowth process must therefore be concerned. Our calculation was further extended to the case of c-GaN stripes with upside down trapezoidal cross section. As observed experimentally, the stripes had rather planar top surfaces. To explain such feature, our calculation suggested that in such a case *L* must be high, while the *weight* must be small. Also, c-GaN with high purity was predicted at the growth condition with higher *L*.

According to our simulation, mechanism of cubic-to-hexagonal structural phase transition is suggested as an incentive of the surface concentration profiles.

# References


[1] Miyajima T., Tojyo T., Asano T., Yanashima K., Kijima S., Hino T., Takeya M., Uchida S., Tomiya S., Funato K., Asatsuma T., Kobayashi T. and Ikeda M. GaN-based blue laser diodes. Journal of Physics: Condensed Matter **13** (2001): 7099-7114.

[2] Bandic Z. Z., Piquette E. C., Bridger Beach, P. M., Keuch T. F. and McGill T. C. Nitride based high power devices: design and fabrication issues. Solid-State Electronics **42** (1998): 2289-2294.

[3] Yanagihara M., Uemoto Y., Ueda, T., Tanaka T. and Ueda D. Recent advances in GaN transistors for future emerging applications. Physica Status Solidi (a) **206** (2009): 1221-1227.

[4] As D. J. and Lischka K. Heteroepitaxy of doped and undoped cubic group III-nitrides. Physica Status Solidi **176** (1999): 475-485.

[5] Brazis R. and Raguotis R. Monte Carlo modeling of phonon-assisted carrier transport in cubic and hexagonal gallium nitride. Optical and Quantum Electronics **38** (2006): 339-347.

[6] Widmann F., Simon J., Daudin B., Feuillet G., Rouviere F. L and Pelekanos N. T. Blue-light emission from GaN self-assembled quatun dots due to giant piezoelectric effect. Physical Review B **58** (1998): R15 990-R15 992.

[7] Ahn D. and Park S.-H. Optical gain of strained hexagonal and cubic GaN quantum-well lasers. Applied Physics Letters **69** (1996): 3303-3305.

[8] Kuwano N., Nagatomo Y., Kobayashi, K., Oki K., Miyoshi S., Yaguchi H., Onabe K., and Shiraki Y. Transmission electron microscope observation of cubic GaN grown by metalorganic vapor phase epitaxy with dimethylhydrazine on (001) GaAs. Japanese Journal of Applied Physics **33** (1994):18-22.

[9] Tachibana H., Ishido T., Ogawa M., Funato M., Fujita S. and Fujita S. Relation between GaAs surface morphology and incorporation of hexagonal GaN into cubic GaN. Journal of Crystal Growth **196** (1999): 41-46.

[10] Ogawa M., Funato M., Ishido T., Fujita S. and Fujita S. The role of growth rates and buffer layer structures for quality improvement of cubic GaN grown on GaAs.

Japanese Journal of Applied Physics **39** (2000): L69-L72.

[11] Chichibu S. F., Sugiyama M., Nozaka T., Suzuki T., Onuma T., Nakajuma K., Aoyama T., Sumiya M., Chikyow T. and Uedono A. Reduction of point defect density in cubic GaN epilayers on (001) GaAs substrates using $Al_xGa_{1-x}N$/GaN superlattice underlayers. Journal of Crystal Growth **272** (2004): 481-488.

[12] Sanorpim S., Takuma E., Katayama R., Onaba K., Ishinose H. and Shiraki Y. Reduction of planar defect density in laterally overgrown cubic-GaN on patterned GaAs(001) substrates by MOVPE. Physica Status Solidi (b) **234** (2002): 840-844.

[13] Shen X. M., Fu Y., Feng G., Xhang B. S., Feng Z. H., Wang Y. T. and Yang H. Structural characterization of epitaxial lateral overgrown GaN on patterned GaN/GaAs(001) substrates. Journal of Crystal Growth **246** (2002): 69-72.

[14] Kitamura S., Hiramatsu K. and Sawaki N. Fabrication of GaN hexagonal pyramids on dot-patterned GaN/sapphire substrates via selective metalorganic vapor phase epitaxy. Japanese Journal of Applied Physics **34** (1995): L1184-1186.

[15] Wang Y. D., Zang K. Y. and Chua S. J. Nonlithographic nanopatterning through anadic aluminum oxide template and selective growth of highly ordered GaN nanostructures. Journal of Applied Physics **100** (2006): 054306 1-4.

[16] Hersee S., Sun X. and Wang X. The controlled growth of GaN nanowires. Nano Letters **6** (2006): 1808-1811.

[17] Shen X. M., Feng G., Zhan B. S., Duan L. H., Wang Y. T. and Yang H. Selective area growth of GaN on GaAs(001) substrates by metalorganic vapor-phase epitaxy. Journal of Crystal Growth **252** (2003): 9-13.

[18] Kawaguchi Y., Nambu S., Sone H., Shibata T., Matsushima H., Yamaguchi M., Miyake H., Hiramatsu K. and Sawaki N. Selective area growth of GaN using tungsten mask by metalorganic vapor phase epitaxy. Japanese Journal of Applied Physics **57** (1998): L845-L848.

[19] Kato T., Honda Y., Kawaguchi Y., Yamaguchi M. and Sawaki N. Selective growth of GaN/AlGaN microstructures by metalorganic vapor phase epitaxy. Japanese Journal of Applied Physics **40** (2001): 1806-1898.

[20] Dupuis R. D., Park J., Grudowski P. A., Eiting C. J., Liliental-Weber Z. Selective-area and lateral epitaxial overgrowth of III-N materials by metalorganic chemical vapor

deposition. Journal of Crystal Growth **195** (1998): 340-345.

[21] Setiagung C., Wu J., Onabe K. and Shiraki Y. Selective area growth of GaN and fabrication of GaN/AlGaN quantum wells and grown facets. Physical Status Solidi (a) **188** (2001): 719-723.

[22] Bhat I. and Zhang R. Anisotropy in selective metalorganic vapor phase epitaxy of CdTe on GaAs and Si substrates. Journal of Electronic Materials **35** (2006): 1293-1298.

[23] Coltrin M. E. and Mitchell C. C. Mass transport and kinetic limitations in MOCVD selective-area growth. Journal of Crystal Growth **254** (2003): 35-45.

[24] Sugiyama M., Waki N., Nobumori Y., Song H., Nakano T., Arakawa T., Nakano Y. and Shimogaki Y. Control of abnormal edge growth in selective area MOVPE of InP. Journal of Crystal Growth **287** (2006) 668-672.

[25] Gibbon M., Stagg J.P., Cureton C.G., Thrush E.J., Jones C.J., Mallard R.E., Pritchard R.E., Collis N. and Chew A. Selective-area low-pressure MOCVD of GaInAsP and related materials on planar InP substrates. Semiconductor Science and Technology **8** (1993): 998-1010.

[26] Greenspan J. E., Zhang X., Puetz N. and Emmerstorfer B. Growth mechanisms and modeling for metalorganic chemical vapor deposition selective-area epitaxy on InP substrates. The Journal of Vacuum Science and Techonology A **18** (2000): 648-651.

[27] Shioda T., Sugiyama M., Shimogaki Y. and Nakano Y. Vapor phase diffusion and surface diffusion combined model for InGaAsP selective area metal-organic vapor phase epitaxy. Journal of Crystal Growth **298** (2007): 37-40.

[28] Stringfellow G.B. A critical appraisal of growth mechanisms in MOVPE. Journal of Crystal Growth **68** (1984): 111-122.

[29] Stringfellow G.B. Development and current status of organometallic vapor phase epitaxy. Journal of Crystal Growth **264** (2004): 620-630.

[30] Sugiyama M., Oh H-j., Nakano Y., and Shimogaki Y., Polycrystals growth on dielectric masks during InP/GaAs selective MOVPE. Journal of Crystal Growth **261** (2004): 411-418.

[31] Dupuis N., Decobert J., Lagree P.-Y., Lagay N., Poingt F., Kazmierski C., Ramdane A. and Ougazzaden A. Mast pattern interference in AlGaInAs selective area metal-organic vapor-phase epitaxy: experimental and modeling analysis. Journal of Applied

Physics **103** (2008): 113113

[32] Fujii T., Ekawa M. and Yamazaki S. Growth pressure dependent of selective area metalorganic vapor phase epitaxy on planar patterned substrates. Journal of Crystal Growth **156** (1995): 59-66.

[33] Shioda T., Tomita Y., Sugiyama M., Shimogaki Y. and Nakano Y. GaN selective area metal-organic vapor phase epitaxy: prediction of growth rate enhancement by vapor phase diffusion model. Japanese Journal of Applied Physics **46** (2007): L1045-L1047.

[34] Greenspan J. E., Alloy composition dependence in selective area epitaxy on InP substrates. Journal of Crystal Growth **236** (2002): 273-280.

[35] Alam M.A., People R., Isaacs E., Kim C.Y., Evans-Lutterodt K., Siegrist T., Pernell T.L., Vandenberg J., Sputz S.K., Chu S.N.G., Lang D.V., Smith L. and Hybertsen M.S. Simulation and characterization of the selective area growth process. Applied Physics Letters **74** (1999): 2617-2619.

[36] Ida M., Shigekawa N., Furuta T., Ito H., Kobayashi T. Compositional change near the mask edge in selective InGaAs growth by low-temperature MOCVD. Journal of Crystal Growth **158** (1996): 437-442.

[37] Wu J., Kudo M., Nagayama A., Yaguchi H., Onabe K. and Shiraki Y. Selective growth of cubic GaN on patterned GaAs(100) substrates by metalorganic vapor phase epitaxy. Physica Status Solidi (a) **176** (1999): 557-560.

[38] Sanorpim S., Takuma E., Katayama R., Onabe K., Ichinose H. and Shiraki Y. Laterally overgrown GaN on patterned GaAs(001) substrates by MOVPE. Physica Status Solidi (a) **192** (2002): 446-452.

[39] Sanorpim S., Wu J., Onabe K. and Shiraki Y. Effects of growth temperature in selective-area growth of cubic GaN on GaAs(100) by MOVPE. Journal of Crystal Growth 237-**239** (2002): 1124-1128.

[40] Greenspan J.E., Blaauw C., Emmerstorfer B., Glew R.W. and Shih I. Analysis of a time-dependent supply mechanism in selective area growth by MOCVD. Journal of Crystal Growth **248** (2003): 405-410.

[41] Eversteyn F.C., Severin P.J.W., Brekel C.H.J.v.d. and Peek H.L. A stagnant layer model for the epitaxial growth of silicon from silane in a horizontal reactor. Journal of The Electrochemical Society: Solid State Science **117** (1970): 925-931.

[42] Shioda T., Sugiyama M., Shimogaki Y. and Nakano Y. Selective area metal-organic vapor-phase epitaxy of InN, GaN and InGaN covering whole composition range. Journal of Crystal Growth **311** (2009): 2809–2812

[43] Langmuir I. The adsorption of gases on plane surfaces of glass, mica and platinum. Journal of the American Chemical Society **40** (1918): 1361-1403.

[44] Present R.D. Kinetic theory of gases. New York: McGraw-Hill, 1958.

[45] Nakamura S. Applied numerical methods in C. New Jersey: PTR Prentice-Hall, Inc., 1993.

[46] Fu Y., Yang H., Zhao D.G., Zheng X.H., Li S.F., Sun Y.P., Feng Z.H., Wang Y.T. and Duan L.H. Epitaxial lateral overgrowth of cubic GaN by metalorganic chemical vapor deposition. Journal of Crystal Growth **225** (2001): 45-49.

[47] Lebedev V., Tonisch K., Niebelschutz F., Cimalla V., Cengher D., Cimalla I., Mauder Ch., Hauguth S. and Ambacher O. Coalescence aspects of III-nitride epitaxy. Journal of Applied Physics **101** (2007): 054906.

# APPENDICES

# APPENDIX A

## INTERNATIONAL SCIENTIFIC PAPER

pss-Header will be provided by the publisher



# A growth model of cubic GaN micro-stripes grown by MOVPE: vapor phase diffusion model including surface migration effects

**Pitsiri Sukkaew[1], Sakuntam Sanorpim[*,1,2] and Kentaro Onabe[3]**

[1] Department of Physics, Faculty of Science, Chulalongkorn University, Phayathai Rd., Pathumwan, Bangkok 10330, Thailand
[2] Center of Innovative Nanotechnology, Chulalongkorn University, Phayathai Rd., Pathumwan, Bangkok, 10330 Thailand
[3] Department of Advanced Materials Science, The University of Tokyo, 5-1-5 Kashiwanoha, Kashiwa 277-8561, Japan

Received ZZZ, revised ZZZ, accepted ZZZ
Published online ZZZ (Dates will be provided by the publisher.)

**PACS** 81.05.Ea, 81.10.Aj, 81.15.Aa, 81.15.Kk

* Corresponding author: e-mail sakuntam.s@chula.ac.th, Phone: +66 2 218 7541, Fax: +66 2 253 1150

Growth features of c-GaN stripes grown by selective area metalorganic vapour phase epitaxy (SA-MOVPE) on GaAs (001) substrates with stripe patterns aligned along [110] direction were analyzed by vapour phase diffusion (VPD) model including surface migration effects from (111) facets. An addition of surface migration effects was found to improve the correlation between the simulation and experiment for the fill factors smaller than 0.5. The effects of the surface migration length ($L$) and the weight of surface migration contribution on the surface profile and the growth rate of the c-GaN stripes were also analyzed. An increase of $L$ was found to strongly enhance the growth rate at the center of c-GaN stripes, while increasing the weight of contribution leads to the growth rate enhancement at the edges of the stripes. Our simulation demonstrated that the most probable values of $L$ and the weight of contribution were 0.8 μm and 0.13, respectively. According to our simulation, mechanism of cubic-to-hexagonal structural phase transition is suggested as an incentive of the surface concentration profiles.



**1 Introduction** GaN and related alloys are receiving considerable attention not only for their applications in blue-UV optoelectronic devices but also for their potential for electronic devices operating under extreme conditions [1]. When crystallizing in cubic structure, the crystal is predicted to have superior electrical properties, such as lower resistivity, lower electron effective mass and higher doping efficiency [2, 3]. However, to acquire such assets, the crystal quality is mandatory. We demonstrated that selective area metalorganic vapour phase epitaxy (SA-MOVPE) can lessen the planar defect density in cubic GaN (c-GaN) [4, 5], which resulted from a large lattice mismatch (~20%) between c-GaN and GaAs substrate. However, in this method structural phase transition of the crystal from cubic to hexagonal was found with the presence of (111)B facets [6]. Moreover, the growth features also depend on mask stripe alignment [6, 7], and fill factor – the ratio of opening width to the pattern period [8]. Therefore, to control the growth feature and quality of SA c-GaN films, an insight understanding of selective area growth mechanism is required.

In our previous work [9], we showed that the vapour phase diffusion (VPD) model with $D/k$, an effective gas phase diffusion length, of 15 μm could analyze the growth rate of narrow stripe SA c-GaN for fill factor higher than 0.5, but underestimate the result for lower fill factors. To improve, in this work, surface migration effects from the appearance of no-growth (111) facets were added into the previous results. The newly resulted growth rate profiles were analyzed as a function of fill factor and compared with the results from the VPD model.

**2 Experiment** SA c-GaN films were grown on GaAs (001) substrates, which were patterned by stripes of dielectric mask aligned in the [110] direction with 4.2 μm fixed mask width. The opening areas were varied to control fill factors, which ranged from 0.35 to 1.0 (no mask). All samples were grown by MOVPE with trimethylgallium (TMGa) and dimethylhydrazine (DMHy) as the precursors

of Ga and N, respectively. After growing 100 nm-thick GaAs and 20 nm-thick c-GaN buffer layers at 700°C and 600°C, c-GaN layer was grown at 900°C for 15 min. Growth features of c-GaN stripes with fill factor 0.35, 0.48, and 0.58 are shown in Figs. 1(a)-1(c). More details of preparation and growth were reported elsewhere [3].

**3 Modelling** The growth mechanism of SA c-GaN stripes might be explained by two-step growth shown in Fig. 1(d). In the first step, the film would grow directly on the opening region of the substrate surface. During this step, its shape was believed to be a trapezoid with two (111)B sidewalls, indicated as white dashed lines in Figs. 1(a)-1(c). In this stage, the growth rate of (111)B facets was assumed to be very low until the length of the facet exceeded the surface diffusion length of the Ga precursor [10]. The second step, namely lateral growth, would begin when the length of the (111)B facets exceeded the diffusion length of Ga precursor on the (111)B surface, which resulted in both lateral growth and vertical growth. Without disturbance, this stage would continue until coalescence.

The probability of the two-step growth was supported by our previous experimental results [5, 6, 9]. Firstly, as shown in Figs. 1(a)-1(c) [9], the (111)B facets can be seen apparently as sidewalls of the c-GaN stripes. Secondly, transmission electron microscopy (TEM) analysis of SA c-GaN films grown at the same growth conditions [5, 6] showed that the films possessed cubic structure only in the trapezoidal region (region I, the first step growth) above the opening substrate surface which was bounded by (111)B sidewalls. For the lateral growth region (region II, the second step growth), which started from the (111)B facets, the crystal structure was shown to be hexagonal phase. This difference in crystal structure suggested two different growth processes. To analysis the growth features of c-GaN stripes just only on the opening regions, we therefore ignored the lateral growth.

During the first step growth, the Ga precursors adsorbed on the (111)B stable facet can either migrate further to the (001) top surface or desorb away. This model gives many unknown parameters i.e. firstly the surface migration length on (001) facet, $L$, which represents the distance that Ga precursors can migrate from the edge to the inner region of (001) top surface, secondly the probability constant that a Ga precursor would be adsorbed on the (111) facets and lastly the partial pressure of the Ga precursors above the facets, which was assumed constant and position independent. To simplify, the two latter parameters were combined and interpreted as the weight of surface migration contribution, called shortly as the weight of contribution.

According to the model, an extent of surface migration contribution was found to depend on the length of (111) facets for the case that the length of (111) facets did not exceed the surface migration length of the Ga precursor on the (111) facet, defined as $L(111)$. Otherwise, the extent of surface migration contribution would depend instead on

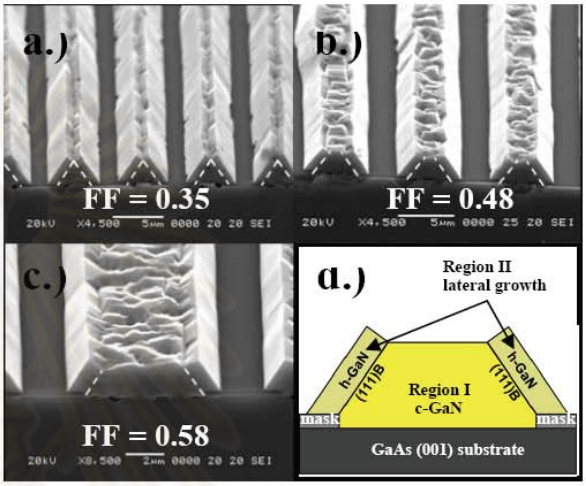


**Figure 1** Bird's eye view scanning electron microscopy (SEM) images of c-GaN films on GaAs (001) substrate

$L(111)$. To simplify, since we interest in the growth rate of the film when no lateral growth occurs, the length of (111) facets was assumed to be less than the value of $L(111)$, which means that no accumulation of the precursors could exist anywhere on the (111) facets.

The length of (111) facets used in our work was computed from the thickness at the centre of the (001) top surface. Firstly, we started to contribute the effect of surface migration from the thickness calculated using VPD model with $D/k$ value of 15 μm [9]. From these initial values, the growth profile as a function of fill factors from VPD model including surface migration was simulated and from this growth profile the new value of the height was calculated. The new height would be used via an iteration technique for the calculation of the growth rate profile. The iteration was continued until the growth profile saturated.

**4 Results and discussion** Figure 2 shows the normalized thickness profiles obtained from VPD model with and without contribution of surface migration effects. For comparison, the normalized thickness profiles measured from the grown samples is also illustrated. The contribution of surface migration effect can improve the growth rate for small fill factors (<0.5), in which the results from the VPD model deviates from the experiment (see blue solid line). By adjusting the values of surface migration length on the (001) surface, $L$, and the weight of contribution, the most probable values of $L$ and weight of contribution were found to be 0.8 μm and 0.13, respectively, as illustrated in Fig. 2 (see black solid line).

In order to understand the effect of surface migration on the VPD model, the surface diffusion length $L$ and the weight of contribution were analyzed as a function of fill factor. The simulated results were shown in Fig. 2. In Fig. 2(a), value of $L$ was varied from 0.5 to 2.0 μm, while the weight of contribution was maintained at 0.13. On the

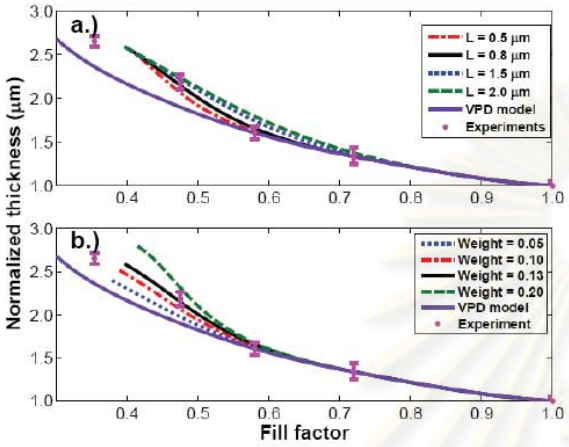


**Figure 2** Growth rate profiles from VPD model with and without surface migration: (a) varying $L$ and fixed weight at 0.13 and (b) varying weight and fixed $L$ at 0.8 μm.

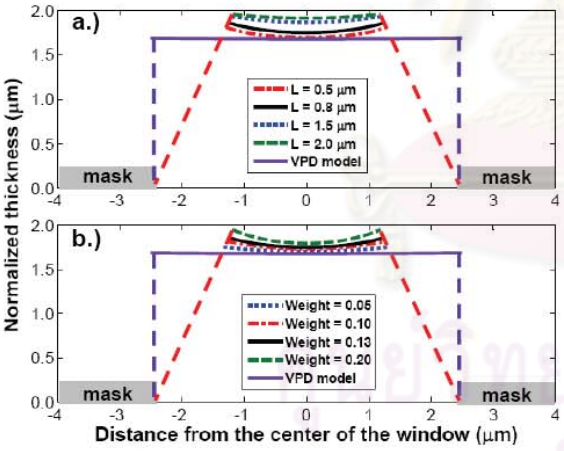


**Figure 3** Surface profiles at fill factor 0.55 from VPD model with and without surface migration: (a) varying $L$ and fixed weight at 0.13 and (b) varying weight and fixed $L$ at 0.8 μm.

other hand, in Fig. 2(b), the value of $L$ was kept at 0.8 μm, while the weight of contribution was varied from 0.05 to 0.20. It should be noted that all growth rate profiles computed from VPD model with surface migration effects terminates at some small values of fill factor. Such terminated points are at the fill factor where the two sidewall facets merge together and thus only lateral growth will be permitted thereafter.

As shown in Figs. 2(a) and 3(a), an increase of $L$ leads to a greater amount of Ga precursors reaching the center of the opening area and in turn increases the growth rate everywhere on the (001) top surface. Considering at one fill factor, the increasing of $L$ also leads to a higher growth rate enhancement at the center of the opening area. However, no influence of $L$ was observed on the terminated points where the two sidewall facets merged. This phenomenon results from the fact that greater $L$ gives the precursors higher mobility to diffuse along the (001) growing surface. A trapezoid shape with (001) planar top surface, which is a proper shape for the formation of cubic structure, is therefore expected with increasing of $L$.

Effect of the weight of contribution on the growth rate enhancement profiles is shown in Figs. 2(b) and 3(b). Increasing weight of contribution leads to higher growth rate enhancement for SA c-GaN with small fill factors. The increasing also leads to a greater amount of Ga precursors accumulating at the edges of the (001) top surface. Such surface concentration profile is believed to induce the structural phase transition of GaN from cubic to hexagonal phase, observed in region II (Fig. 1(d)).

**5 Conclusion** We have analyzed the growth rate of SA c-GaN films on GaAs (001) substrates through VPD model including surface migration effects from the presence of the stable (111) sidewalls. An introduction of surface migration was found to improve the simulated results from the VPD model of SA c-GaN films for small fill factors, which firstly deviated from experiments. Two new parameters (i.e. the surface diffusion length on (001) plane and the weight of contribution) resulted from the addition of surface migration effect were found to be essential for the structural phase control of c-GaN selective area growth.

**Acknowledgements** This work was partly supported by Office of the National Research Council of Thailand (NRCT), by Science and Technology Innovation Support Grant, Chulalongkorn University, by the Development and Promotion for Science and Technology Talents Project (DPST) and Graduated School, Chulalongkorn University.

## References

[1] D. J. As, Microelectr. J. **40**, 204 (2009).
[2] H. Okunuma, K. Ohta, G. Feuillet, K. Balakrishnan, S. Chichibu, H. Hamaguchi, P. Hacke and S. Yoshida, J. Cryst. Growth **178**, 113 (1997).
[3] J. Wu, H. Yaguchi, K. Onabe, Y. Shiraki, and R. Ito, Jpn. J. Appl. Phys. **37**, 1440 (1998).
[4] Yi Fu, Hui Yang, D.G. Zhao, X.H. Zheng, S.F. Li, Y.P. Sun, Z.H. Feng, Y.T. Wang and L.H. Duan, J. Cryst. Growth **225**, 45 (2001).
[5] S. Sanorpim, E. Takuma, H. Ichinose, R. Katayama and K. Onabe, Phys. Status Solidi B **244**, 1769 (2007).
[6] S. Sanorpim, E. Takuma, K. Onabe, H. Ichinose and Y. Shiraki, Phys. Status Solidi A **192**, 446 (2002).
[7] X.M. Shen, G. Feng, B.S. Zhang, L.H. Duan, Y.T. Wang and H. Yang, J. Cryst. Growth **252**, 9 (2003).
[8] S. Sanorpim, J. Wu, K. Onabe and Y. Shiraki, J. Cryst. Growth **237-239**, 1124 (2002).
[9] P. Sukkaew and S. Sanorpim, submitted to "International Conference on Nanoscience & Technology" ChinaNANO, China, Beijing (2009).
[10] J. E. Greenspan, C. Blaauw, B. Emmerstorfer, R. W. Glew and I. Shih, J. Cryst. Growth **248**, 405 (2003).

# APPENDIX B

# PROCEEDING

การประชุมเสนอผลงานวิจัย ระดับบัณฑิตศึกษาแห่งชาติ ครั้งที่ ๑๔
มหาวิทยาลัยเทคโนโลยีพระจอมเกล้าพระนครเหนือ
วันที่ ๑๐ – ๑๑ กันยายน ๒๕๕๒

## แบบจำลองการแพร่ในสถานะก๊าซสำหรับการปลูกผลึกคิวบิกแกลเลียมไนไตรด์แบบเลือกพื้นที่โดยเอ็มโอวีพีอี

## Vapor Phase Diffusion Model for Selective Area Growth of cubic GaN via MOVPE

พิชญ์สิริ สุกแก้ว[1] และ สกุลธรรม เสนาะพิมพ์[2]

**บทคัดย่อ**

ในงานวิจัยนี้ เราได้ประยุกต์ใช้แบบจำลองการแพร่ในสถานะก๊าซเพื่อวิเคราะห์ฟิล์มบางชนิดคิวบิกแกลเลียมไนไตรด์ซึ่งปลูกผลึกโดยวิธีคัดเลือกพื้นที่ ผ่านกระบวนการเมทอล-ออแกนิกเวเปอร์เฟสเอพิแทกซี (เอ็มโอวีพีอี) ลงบนซับสเตรทซนิดแกลเลียมอาร์เซไนด์ที่ผ่านการสร้างแบบให้มีลักษณะเป็นเส้นแคบในทิศทาง [011] ผลที่ได้จากการจำลองถูกนำมาเปรียบเทียบกับผลการทดลอง ผ่านการสังเกตภาพตัดขวางที่ได้จากกล้องจุลทรรศน์อิเล็กตรอนแบบส่องกราด จากการวิเคราะห์พบว่า พารามิเตอร์ที่บ่งชี้อัตราการปลูกของฟิล์ม ได้แก่ ค่าอัตราส่วน $D/k$ และตัวประกอบเติมเต็ม (fill factor) ซึ่งเป็นอัตราส่วนระหว่างความกว้างของบริเวณเปิดบนผิวซับสเตรทต่อคาบของแบบ นอกจากนี้พบว่า ที่อัตราส่วน $D/k$ เป็น 15 μm แบบจำลองการแพร่ในสถานะก๊าซสามารถอธิบายผลการทดลองในช่วงตัวประกอบเติมเต็มมากกว่า 0.5 ได้เป็นอย่างดี สำหรับตัวประกอบเติมเต็มที่มีค่าน้อยกว่า 0.5 บ่งชี้ถึงความจำเป็นในการเพิ่มอิทธิพลของไมเกรชันบนผิว

**Abstract**

In this work, the vapor phase diffusion model was applied to analyze the selective area (SA) growth of cubic GaN on a narrow [011]-stripe-patterned GaAs substrate via metalorganic vapor phase epitaxy (MOVPE). Simulation results were compared with the growth results obtained from cross-sectional scanning electron microscopy. It is known that growth rate of SA cubic GaN was parameterized by the value of $D/k$ as well as the fill factor (the ratio of the open width to the pattern period). $D/k$ due to having a dimension of length can thus be interpreted as the effective diffusion length of Ga-precursor on the growing surface. For $D/k$ =15 μm, the vapor phase diffusion model was found to well describe the experimental results for the SA cubic GaN layers with the fill factors greater than 0.5. For lower fill factors, the surface migration effects are needed.

**คำสำคัญ** : แบบจำลองการแพร่ในสถานะก๊าซ, การปลูกแบบคัดเลือกพื้นที่, คิวบิกแกลเลียมไนไตรด์, อัตราการปลูก

**Keywords** : vapor phase diffusion model, selective area growth, cubic GaN, growth rate

1 นิสิตหลักสูตรวิทยาศาสตรมหาบัณฑิต สาขาวิชาฟิสิกส์ ภาควิชาฟิสิกส์ คณะวิทยาศาสตร์ จุฬาลงกรณ์มหาวิทยาลัย
2 ผู้ช่วยศาสตราจารย์ ดร. ภาควิชาฟิสิกส์ คณะวิทยาศาสตร์ จุฬาลงกรณ์มหาวิทยาลัย

The 14th National Graduate Research Conference
King Mongkut's University of Technology North Bangkok
September 10–11, 2009

**Introduction**

Cubic GaN, c-GaN, when compared with hexagonal GaN, h-GaN, exhibits several of attractive advantages, such as higher electron and hole mobilities, easier p-type doping, easier cleaving and easier contacting [1]. For growing epitaxial c-GaN films, metalorganic vapor phase epitaxy (MOVPE) has been widely used owing to its applicability in mass production. For high performance electronic-photonic device fabrication where the deposition is usually required only on predetermined areas of the substrate, but strictly prohibited elsewhere, the selective area (SA) technique is usually applied in combination with MOVPE. In this technique, the unwanted area will be covered with thin layer of dielectric material, usually called "mask", so that, when using this technique with proper growth condition, nucleation will occur only on the exposed substrate surface, usually called "window", where the basis atoms arrange themselves in a highly ordered structure.

In order to predict the growth rate and morphologies of the growing films, a model for computer simulation is needed. In SA-MOVPE, two transportation mechanisms are believed to involve: vapor phase diffusion and surface migration. However, the answer of which mechanism dominates depends on the SA pattern dimension. For the case of wide SA pattern, in which the stripe width is greater that 10 μm, Gibbon *et al.* [2] found that vapor phase diffusion dominated and also suggested the neglect of surface migration. From this discovery, they designed the well-known vapor phase diffusion model to predict the thickness of the growing films. The wide stripe case has been widely studied also by others using vapor phase diffusion model [3-7]. However, in the case of narrow SA patterns, in which the stripe width is only a few micrometers, the vapor phase diffusion model seemed to have failed if surface migration effects had not been included [8].

In our work, we considered the result of vapor phase diffusion model for both wide and narrow stripe patterns. These calculation results were compared and discussed in details. Finally, the calculation results for the case of narrow stripes with 4.2 micrometer mask width were compared with experimental results of c-GaN films.

**Materials and methods**

**I. Growth Experiment**

The c-GaN films were selectively grown by MOVPE on a stripe-patterned GaAs (100) substrate which was partially covered by dielectric stripes aligned periodically along the [011] direction of the substrate surface. The films were grown under low pressure of 160 Torr. DMHy and TMG were used as the sources of N and Ga precursors, respectively. The flow rate of TMG, carrier gas, growth temperature and V/III ratio were 8 sccm, $H_2$, 900°C and 25, respectively. The mask material being used here was $SiN_x$ with the width fixed at 4.2 μm. The stripes were aligned periodically with different pattern periods labeled by fill factors, W/(W+M), where W and M were window width and mask width, respectively. The SA-grown films were found to have good selectivity; no deposition on mask was observed. The SEM images of the films at fill factors 0.35, 0.48 and 0.58 were shown in Fig. 1.

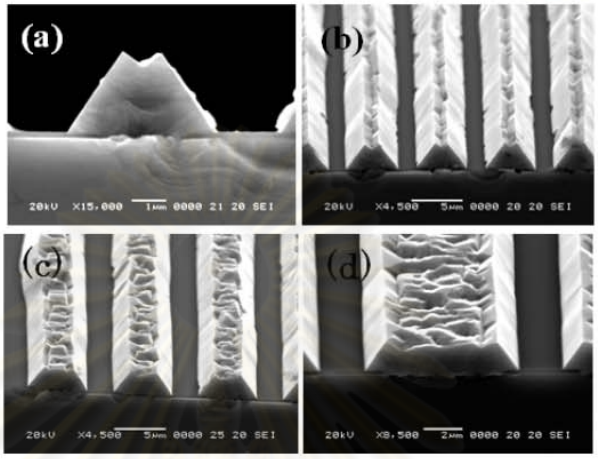


**Fig. 1** (a) Cross-sectional SEM images for c-GaN on stripe patterns with fill factor of 0.35 and (b-d) bird's eye view SEM images for c-GaN on stripe patterns with fill factor of 0.35, 0.48 and 0.58 respectively.

**II. Simulation: Vapor phase diffusion model**

Gibbon *et al.* [2] had designed the vapor phase diffusion model and found an interesting result that the film thickness profile could be deduced from the profile of group III concentration on the substrate surface. In this model, the group III concentration was calculated from a steady state diffusion equation in a stagnant layer subjected to a proper boundary condition in which many assumptions and simplifications had been made. A schematic illustration of the vapor phase diffusion model for the growth of SA c-GaN is shown in Fig. 2. The area above substrate surface in the figure is assumed to be stagnant, i.e. no forced convection. Thus, the group III (Ga) concentration ( $u$ ) satisfies the steady state diffusion equation with no source term, $\Delta\mu$=0. The left and right boundary lines are at the center of the two adjacent mask stripes and imposed the condition of no lateral flux of the Ga concentration due to

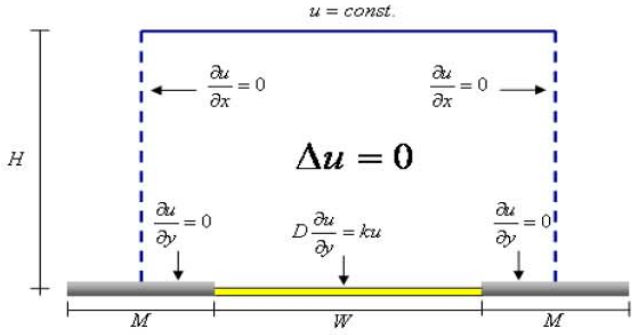


**Fig. 2** Boundary conditions used in the vapor phase diffusion model

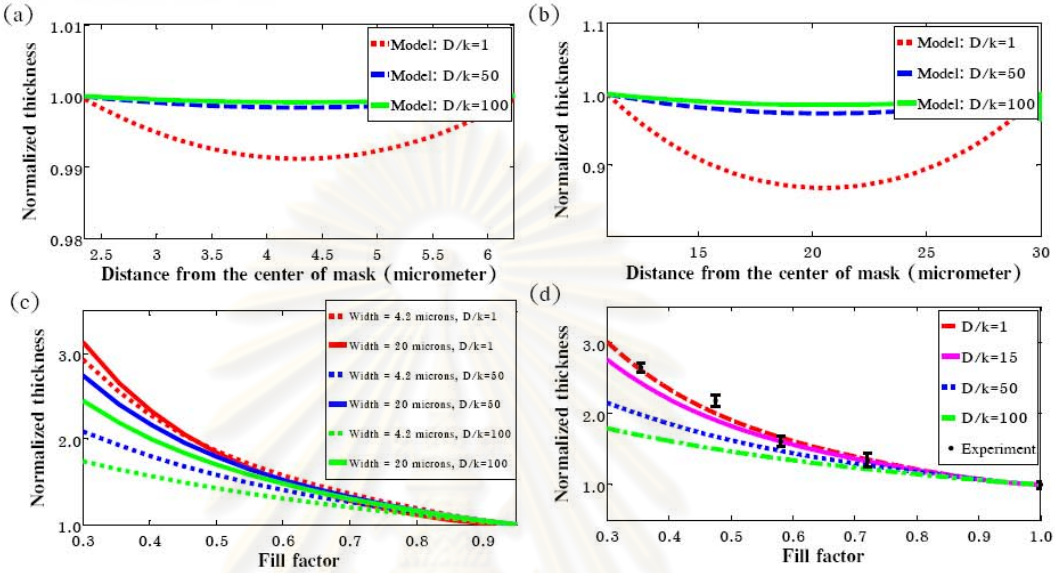


**Fig. 3** (a) Varied $D/k$ with film thickness variation at fill factor 0.5 and mask width 4.2 μm, (b) Varied $D/k$ on film thickness variation at fill factor 0.5 and mask width 20 μm, (c) Calculation result of varied $D/k$ for mask width 4.2 and 20 μm at varied fill factors, (d) Calculation result of varied $D/k$ for mask width 4.2 micrometer at each fill factor compared with experiment.

symmetry, $\partial u/\partial x = 0$. On the surface of the window, the condition of continuous flux is applied in according to Langmuir isotherm [9] and Fick's law. This results in $D\,\partial u/\partial y = ku$ where $D$ and $k$ are diffusion coefficient and rate constant, respectively. On the surface of the masks, since no growth is assumed, we obtain $\partial u/\partial y = 0$. Above the stagnant layer, the Ga precursor concentration is assumed constant. The height of the stagnant layer $H$ used in our case is 1,000 μm where the value of $H$ must be high enough that it does not affect the concentration trend on substrate surface. In our calculation, the finite different method had been used.

**Results and discussion**

The vapor phase diffusion model described in the previous section was applied to simulate the thickness profile of SA c-GaN on [011] stripe patterned GaAs (100) substrates. Firstly, the calculation is performed under the conditions of no mask on the substrate surface (mask width was zero). The height of stagnant layer ($H$) was set to 1000 μm. The constant concentration of the precursor above the stagnant layer was 5 and the value of $D/k$ was varied as 1, 50 and 100 μm.

The simulated film surface was found to have a smooth and positioning-independent-thickness as it is expected. Variation of $D/k$ was found to have profound effects on the simulated film thickness in such a way that increasing $D/k$ results in higher film thickness. Since an increase in $D/k$ while $k$ was kept constant indicates the enhancement of diffusion constant $D$, this suggests that the higher thickness results from greater amount of precursors reaching the substrate surface. Figures 3 (a) and 3 (b) show

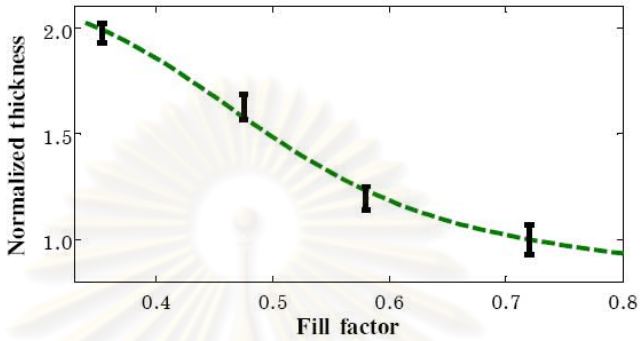


**Fig. 4** A possible trend for the experimental data (bars), showing a well agreement between the simulation (dashed line) adding the surface migration effect and experimental data.

the effect of $D/k$ over the surface profiles of SAG c-GaN films with 4.2 and 20 micrometer mask width, respectively. The simulation condition being used here is the same as no mask condition described above. In these figures, the normalized thickness was defined as the thickness at one position divided by the thickness at the edges of the mask. These figures show that an increase in $D/k$ results in less thickness variation on the film surfaces which implies that an enhancement of $D/k$ results in an increase of the precursor mobilities on the surface. Therefore, increasing $D/k$ gives smoother film surface. $D/k$ ratio, due to having a dimension of length, can thus be interpreted as the effective diffusion length of the Ga precursors. Since in mass transported limit the diffusion constant, $D$, depends more strongly on growth temperature than the rate constant, $k$, smoother film surface can then be obtained at higher growth temperature.

It should be noted that the amount of thickness variation on the surface of narrow stripe pattern is very small compared with the overall film thickness such that the roughness can be ignored. However, for wide stripe the amount of thickness variation is quite large compared with overall film thickness. Thus, the thickness variations on the surface of wide stripe pattern are more sensitive to the value of $D/k$ than that of the narrow stripe. We can then deduce that for narrow stripe pattern small $D/k$ is enough for the precursors to move on the surface, so they can spread themselves more smoothly.

Figure 3 (c) shows the effect of $D/k$ and fill factors on the normalized thickness at the center of the window of wide and narrow stripe patterns. In this figure, the normalized thickness was the thickness at the center of the window at one fill factor normalized by the thickness at the center of the window of fill factor 0.95. It can be seen that varying $D/k$ has more effect on narrow stripe pattern, while the variation of fill factors has more effect on wide stripe pattern.

Figure 3 (d) shows the calculation results compared with experiments where the mask width was 4.2 μm. It can be seen that the vapor phase diffusion model with $D/k = 15$ μm can describe narrow stripe with good accuracy for the fill factor greater than 0.5. For lower fill factors, however, it predicts lower amount than the experimental results. This suggests that surface migration effect contribution is

needed in this range of fill factors. By considering the entire experimental results it is possible for another trend as shown in Fig. 4.

**Conclusions**

The vapor phase diffusion model was applied to analyze the growth rate of SA c-GaN layers grown on [011] stripe patterned GaAs (100) substrates via MOVPE. The results were found to be parameterized by $D/k$ and fill factor. As increasing of $D/k$, a less thickness variation on the surface of the film was observed. This suggests that an enhancement of $D/k$ increases the distance that Ga precursor moving along the growing surface. Thus, $D/k$, which has a dimension of length, can be interpreted as the effective diffusion length of the precursor. We demonstrated that the vapor phase model with $D/k = 15$ μm is useful to describe the experimental results for the SA c-GaN layers with the fill factors higher than 0.5. For lower fill factors, the surface migration effect should be added.

**Acknowledgement**

This work was partly supported by Office of the National Research Council of Thailand (NRCT) and by Science and Technology Innovation Support Grant, Chulalongkorn University. One of the authors (P.S.) has been supported by Development and Promotion for Science and Technology Talents Project (DPST) and Graduated School, Chulalongkorn University.

**References**

[1] J. W. Orton, and C. T. Foxon, Rep. Prog. Phys. 61 (1998) 1-75.

[2] M. Gibbon, J. P. Stagg, C. G. Cureton, E. J. Thrush, C. J. Jones, R. E. Mallard, R. E. Pritchard, N. Collis and A Chew, Semicond. Sci. Technol. 8 (1993) 998-1010.

[3] T. Shioda, Y. Tomita, M. Sugiyama, Y Shimogaki and Y. Nakano, Jpn. J. Appl. Phys. 46 No.43 (2007) L1045-L1047.

[4] N. Dupuis, J. Decobert, P.-Y. Lagree, N. Lagay, D. Carpentier, F. Alexandre, J. Cryst. Growth. 310 (2008) 4795-4798.

[5] N. Dupuis, J. Decobert, P.-Y. Lagree, N. Lagay, F. Poingt, C. Kazmierski, A. Ramdane, and A. Ougazzaden, J. Appl. Phys. 103, 113113 (2008).

[6] J. Decobert, N. Dupuis, P.Y. Lagree, N. Lagay, A. Ramdane, A. Ougazzanden, F. Poingt, C. Cuisin, C. Kasmierski, J. Cryst. Growth. 298 (2007) 28-31.

[7] M. A. Alam, R. People, E. Isaacs, C. Y. Kim, K. Evans-Lutterodt, T. Siegrist, T. L. Pernell, J. Vandenberg, S. K. Sputz, S. N. G. Chu, D. V. Lang, L. Smith and M. S. Hybertsen, Appl. Phys. Lett. 74 (18), 1999, 2617.

[8] J. E. Greenspan, C. Blaauw, B. Emmerstorfer, R. W. Glew and I. Shih, J. Cryst. Growth. 248 (2003) 405-410.

[9] G. B. Stringfellow, Organometallic Vapor Phase Epitaxy: Theory and Practice, Academic Press, Boston, MA, 1998.

# APPENDIX C

## CONFERENCE PRESENTATIONS

[1] **Sukkaew P.** and Sanorpim S. Growth rate analysis of selective area growth of c-GaN under MOVPE via a vapor phase diffusion model, *4th Siam Physics Congress (SPC2009): physics for dynamic society, Thailand (2009)* (Poster).

[2] **Sukkaew P.** and Sanorpim S. Modeling analysis of growth rate enhancement in selective area growth of c-GaN under MOVPE via a vapor-phase diffusion model, *The Science Forum 2009, Chulalongkorn University, Thailand (2009)* (Oral).

[3] **Sukkaew P.**, and Sanorpim S. Vapor phase diffusion model for selective area growth of cubic GaN via MOVPE, *14th National Graduate Research Conference, King Mongkut's University of Technology North Bangkok, Thailand (2009)* (Oral).

[4] **Sukkaew P.** and Sanorpim S. Growth rate analysis of cubic GaN nano/micro-stripes grown by SA-MOVPE via a vapor phase diffusion model, *International Conference on Nanoscience and Technology (ChinaNANO2009), Beijing, China (2009)* (Oral).

[5] **Sukkaew P.**, Sanorpim S. and Onabe K. A growth model of cubic GaN micro stripes grown by MOVPE: vapor phase diffusion model including surface migration effects, *8th International Conference on Nitride Semiconductors (ICNS-8), Jeju, Korea (2009)* (Poster).

# VITAE

Miss Pitsiri Sukkaew was born on April 4, 1985 in Sing Buri, Thailand. She has been a student in the Development and Promotion for Science and Technology Talents Project (DPST). She had received her Bachelor Degree of Science Program in Physics from the Department of Physics, Faculty of Science, Chulalongkorn University in 2006, and continued her Master's study in 2007.

One of her papers has been accepted to be published in an international scientific journal, Physica Status Solidi (a), which has the impact factor of 1.21 (APPENDIX A). The other has been published in the Proceeding of 14th National Graduate Research Conference, Thailand (APPENDIC B). She has also participated two international conferences, as follows:

[1] **Sukkaew P.** and Sanorpim S. Growth rate analysis of cubic GaN nano/micro-stripes grown by SA-MOVPE via a vapor phase diffusion model, *International Conference on Nanoscience and Technology (ChinaNANO2009), Beijing, China (2009)* (Oral)

[2] **Sukkaew P.**, Sanorpim S. and Onabe K. A growth model of cubic GaN micro stripes grown by MOVPE: vapor phase diffusion model including surface migration effects, *8th International Conference on Nitride Semiconductors (ICNS-8), Jeju, Korea (2009)* (Poster)